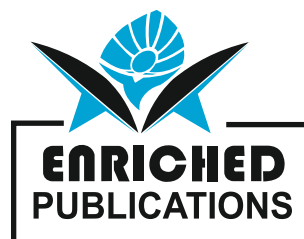


Journal of Surveying and Structural Engineering

Volume No. 12

Issue No. 1

January - April 2024



ENRICHED PUBLICATIONS PVT. LTD

**S-9, IInd FLOOR, MLU POCKET,
MANISH ABHINAV PLAZA-II, ABOVE FEDERAL BANK,
PLOT NO-5, SECTOR-5, DWARKA, NEW DELHI, INDIA-110075,
PHONE: - + (91)-(11)-47026006**

Journal of Surveying and Structural Engineering

Aims and Scope

Journal of Surveying and Structural Engineering is the major new peer-reviewed journal for building surveyors, structural engineers and other professionals concerned with building condition, defects, valuation, repair and maintenance. The Journal's scope encompasses the diverse range of concerns in the survey, appraisal and valuation of the built environment, including –

1. Building surveys
2. Structural surveys
3. Defect investigation
4. Instrumentation and its use
5. Valuation
6. Repairs and maintenance
7. Dilapidations
8. Fit out and refurbishment
9. Building control and building regulations
10. Party wall issues
11. Remedial works
12. Acquisition surveys
13. Insurance assessment and claims
14. Measured surveys
15. Project management and monitoring
16. Sustainable buildings
17. Dispute resolution
18. Professional liability

Journal of Surveying and Structural Engineering

**Managing Editor
Mr. Amit Prasad**

Editor in Chief

Dr. Gupinath Bhandri
Associate Professor
Department of Civil Engineering
Jadavpur University, Kolkata 700032
g.bhandari@civil.jdvu.ac.in

Dr. Ajay Pratap Singh
Maulana Azad National Institute
of Technology, Bhopal
apsmact@gmail.com

Dr. Rakesh Kumar
Maulana Azad National Institute of
Technology, Bhopal
apsmact@gmail.com

Journal of Surveying and Structural Engineering

(Volume No. 12, Issue No. 1, January - April 2024)

Contents

Sr. No.	Title / Authors Name	Pg. No.
1	Design Optimization Of Desilting Chamber By Model Studies – <i>M.K. Verma, M.Z. Qamar, Neena Isaac, Dr. V.V. Bhosekar</i>	01 - 12
2	Numerical Computation for Sizing of Break Pressure Tanks – <i>N.N. Sontake, A.D. Vasudeo, A.D. Ghare, R.N. Ingle</i>	13 - 26
3	Curve Number Derivation For Experimental Plots Of Different Slopes, Hydrologic Soil Groups And Land Uses – <i>Mohan Lal, Surendra Kumar Mishra, Ashish Pandey</i>	27 - 39
4	Static And Dynamic Behaviors Of Geocell Reinforced Soft Clay – <i>Ashim Kanti Dey, Prasenjit Debnath,</i>	40 - 53
5	Trend Analysis of River Yamuna at Two Different Cities through Adaptive Neuro Fuzzy System – <i>Shubhi Bhardwaj</i>	54 - 59

Design Optimization Of Desilting Chamber By Model Studies

M.K. Verma¹, M.Z. Qamar², Neena Isaac³, Dr. V.V. Bhosekar⁴

^{1&2} Scientist 'B', ³ Scientist 'D', ⁴ Scientist 'E'

Central Water & Power Research Station, Pune – 411024 (India)

Email: manoj_rajyog@rediffmail.com,

vvbhosekar@yahoo.co.in

Telephone/Mobile No.: +91 9423209515, 9420176524

ABSTRACT

Desilting chamber is an arrangement in which the flow velocity is reduced by enlarging the channel cross section which forces the suspended sediment to settle at the bottom and is removed through silt flushing tunnels. The water, free from sediment of desired size is in turn carried to the power house through head race tunnel and penstocks for power generation. Various principles and approaches for design of desilting chamber are available but in absence of any definite design specifications in many aspects, its design is conceptualized on the basis of broad guidelines based on past experiences. At this juncture, hydraulic model studies play an important role and are carried out for specific projects wherein; applicability of assumptions and adequacy of design and layout of the desilting arrangements shall be assessed. As desilting chambers are very large underground structures which involve huge financial implications, sometimes comparable to the cost of main dam, proper design can go long way to solve sediment problem in run-of-river hydro power plants. Therefore, to optimize its size required for desired settling efficiency, model study is the only available tool. In addition to sediment removal efficiency, the design of inlet and outlet arrangements as well as flushing arrangement is finalized on the basis of hydraulic model studies. Type of model and scales, suspended sediment simulation, field data requirement for model studies, model limitations, mathematical models and past experience of CWPRS in such studies will be described in this paper.

Keywords: - Desilting chamber, hydraulic model studies, settling efficiency, suspended sediment.

1. INTRODUCTION

Efficient and reliable exclusion of sand and silt has always been one of the main challenges while development of run-of-river hydropower Projects on sediment carrying rivers in Himalayan region. These perennial rivers carry huge quartz rich sediment with them (sometimes 5000 ppm and above in monsoon) and many times it is not possible to remove the sediment in hydropower projects completely which over a period of time drastically reduces the overall efficiency of power generation system. The size and concentration of sediment depends upon the catchment characteristics and vary seasonally. When river water is to be used for hydropower generation, the harmful part of the sediment is to be removed to minimize

minimize the erosion damages to the turbine and other underwater parts of the hydropower plant. In Himalayas, in almost all run-of-river hydropower projects, desilting chambers are provided and is the most effective device for extracting specific particle size for the desired efficiency by adjusting shape and size of the chamber.

A number of approaches for determining the size of chamber are available. These are based on experimental data and on certain assumptions for flow velocity, fall velocity, sediment concentration and its movement. The experience has been that each approach gives a size of desilting chamber quite different from the other for same sediment settling efficiency and design parameters. The settling efficiency in prototype is also dependent on the hydraulics of inlet and outlet transitions as well as on flushing arrangements but no definite design criteria of general application for their design is available. Therefore, preliminary design in each case is tested on physical hydraulic models.

2. NEED FOR DESILTING CHAMBERS

Run-of-river schemes are generally provided with desilting chambers to exclude harmful suspended sediment which passes through the trash rack of power intake into the water conductor system of hydro electric project. Some recommendations / guidelines for the necessity of a desilting chamber are available. The maximum permissible size of sediment particles may range between 0.1 to 0.7 mm depending upon the type of turbine as below (Asthana 2007):

Pelton wheel	0.1 mm
Francis turbine	0.3 to 0.5 mm
Kaplan turbine	0.5 to 0.7 mm

The limit on permissible particle size for medium head plants is 0.5 to 0.2 mm and for high head plant it is 0.1 mm as recommended by (Mosonyi 1965). However, Bharat Heavy Electricals Ltd. who are hydro power equipment manufacturer in India have fixed following guidelines (Acharekar 1978):

- Particles of > 0.25 mm size and hardness > 5 on Mohr's scale are harmful.
- If the concentration of particle is > 200 ppm, desilting measures are required.
- Concentration of harmful particles should be reduced by 85% to 95%.
- Du Tong (1981) has concluded from experimental results that damages take place due to cavitation and the process is accelerated by sediment. He has recommended that if the turbine is likely to be eroded within 5-10 years then, the sediment exclusion measures are necessary and if the life of the turbine works out to be more than 20 years, the sediment exclusion measures can be eliminated.

Thus, it can be concluded that in each case certain limit of sediment concentration and particle size has to be fixed by the designer in consultation with turbine manufacture for provision of sediment exclusion device but no definite guidelines are available.

3. DESIGN APPROACHES

The length of the chamber would depend upon fall velocity of particles, depth of flow and forward velocity of flow in the chamber. Initially, length of the chamber used to be determined by working out the horizontal distance travelled by particles for its settlement from the top layer of flow to the bed of desilting chamber. The amount of sediment load deposited in a settling basin is expressed in terms of the removal efficiency of the basin, which is defined as follows:

$$\eta = \frac{q_{si} - q_{se}}{q_{si}} \quad (1)$$

Where η = basin settling efficiency; and q_{si} and q_{se} are amounts of sediment entering and leaving the basin per unit time.

Empirical and analytical methods of computation of settling basin efficiency have been proposed by Camp, Dobbins, United States Bureau of Reclamation (USBR), Sumer, Mosonyi, Cean et al., Richardson et al. and Garde et al. Some of these methods are based on analyses of extensive laboratory data and serve as practical tools for design (Qamar 2014).

However, in absence of any definite criteria in many aspects, the design of desilting chamber is to be based on a broad guide lines, assumptions and experience. Verification of these assumptions and adequacy of the layout as well as other design aspects is required to be assessed by conducting studies in physical models.

4. NEED FOR MODEL STUDIES

“Experimenting with models seems to afford a ready means of investigating and determining beforehand the effects of any proposed hydraulic structure; a means, after what I have seen, I should feel it madness to neglect before entering upon any costly undertaking”, so says Osborne Reynolds (CBIP 1954). It is often worth to study the performance of small replica or “model” of the system or “prototype” that is to be built, before an expensive engineering project is undertaken. Model studies are made for two purposes viz., in order to avoid costly mistakes and to obtain information that will help in the design of

the prototype. Since, it is comparatively inexpensive to modify the construction of a model, several alternative designs in the model may be tried before adopting a final one; such experiments would be excessively costly if they were undertaken with the full scale system (Verma 2002).

It is only through model experiments and research that improvements in the existing works, safe and economical design and construction of new works and furtherance of knowledge on various aspects of hydraulic engineering can be effected. The view that hydraulic models provide a suitable means of specific solutions of the hydrodynamic equations of motion under a known set of boundary conditions, if it is possible to establish quantitative rules for transferring data, is often held. Further, hydraulic models provide the only means of testing and evolving the final design in case of desilting chambers for optimizing the transition length and length of the desilting chamber, optimizing the flushing discharge, estimation of settling efficiency and estimation of the efficacy of the flushing system.

In case of desilting chambers, the objective of conducting model studies is:

- (I) To identify the critical design parameters of a desilting chamber responsible for its efficient functioning suitable for site specific design.
- (ii) To review the empirical approach of preliminary design.
- (iii) To analyze the model results in view of desired settling efficiency of desilting chamber and its flushing efficacy.

Generally, model studies for desilting chamber are conducted for testing the adequacy / feasibility of the desilting basin for 90% removal of suspended sediment coarser than 0.2 mm and efficacy of flushing tunnel below desilting basin in transporting the settled sediment. The view of prototype and its replica in model for Teesta H.E. Project, Stage V, Sikkim is shown in photo 1.

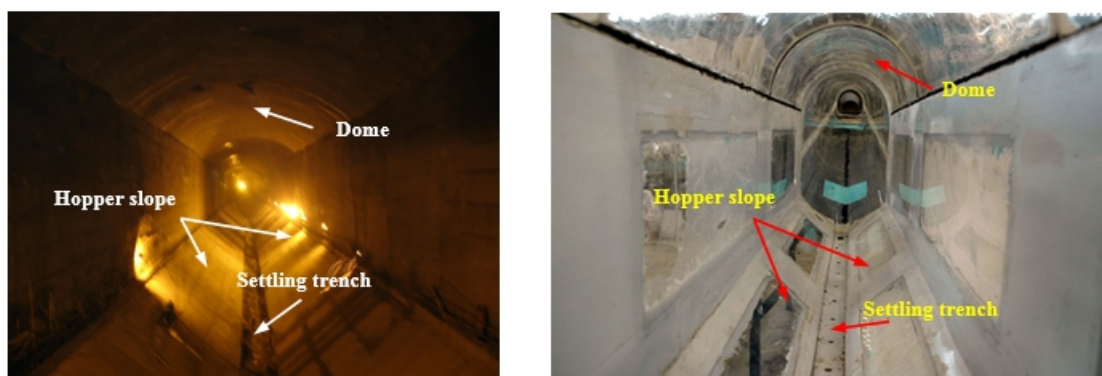


Photo 1 Inside view of chamber in prototype and model

5. TYPE OF HYDRAULIC MODELS AND THEIR SCALES

The scales of such models are determined on similarity of geometry and the Froude's law. Various similitude ratios for a geometrically similar model with Froude's law are as follows;

Let length scale ratio be $L_m/L_p = L_r$ for geometrically similar model. Since Froude Number has to be same in model and prototype.

$$\left(\frac{V^2}{Lg}\right)_m = \left(\frac{V^2}{Lg}\right)_p \quad (2)$$

Since force of gravity is nearly same in model and prototype.

$$\left(\frac{V^2}{L}\right)_m = \left(\frac{V^2}{L}\right)_p \quad (3)$$

This leads to

$$\frac{V_m}{V_p} = \sqrt{\frac{L_m}{L_p}} \quad \text{i.e.} \quad V_r = \sqrt{L_r} \quad (4)$$

From this basic model law other model laws can be derived.

Length scale ratio	=	L_r	
Area scale	=	$(L_r)^2$	
Volume scale	=	$(L_r)^3$	
Velocity scale V_r	=	$(L_r)^{1/2}$	
Therefore, Time Scale T_r	=	Length Scale / Velocity Scale	= $L_r / (L_r)^{1/2} = (L_r)^{1/2}$
Discharge Scale	=	Area Scale x Velocity Scale	= $(L_r)^2 (L_r)^{1/2} = (L_r)^{5/2}$

The scales are based on the availability of cost, space, head and discharge etc. The experience has been that bigger models yield better and more reliable results.

Model studies for desilting chambers are generally conducted in geometrically similar scale rigid bed models for open channel type desilting chambers. In the case of closed conduit type chambers, transparent Perspex/Polycarbonate sheets are used for convenience of fabrication and for visualization of the flow in the chamber. The view of such model is shown in photo 2.

6. SIMULATION OF SEDIMENT

Generally, chambers are designed for removal of sediment coarser than 0.2 mm. For simulation of sediment in the model, a low specific gravity material is required to be used. However, it would not be possible/advisable to go in for very small size of particles of low specific gravity material from the practical considerations. Taking these aspects into consideration, the scales of the models generally vary from 1:20 to 1:30 geometrically similar.

Apart from proper reproduction of design features and inlet and outlet conditions for achieving adequate distribution of flow in the chamber, the accuracy of the results of the model studies would depend upon the realistic simulation of the distribution of the suspended sediment on a vertical which is given by following equation developed by Rouse (1949).

$$\frac{C_y}{C_a} = \left[\frac{d-y}{y} \frac{a}{d-a} \right]^z \quad (5)$$

where.

C_y	=	Concentration at depth "y" above bed level
C_a	=	Concentration at 0.05d above bed level
d	=	Depth of flow
y	=	Depth at which concentration C_y is to be calculated
a	=	0.05d

and $Z = \frac{w}{K \sqrt{g d s}}$

wherein:

w	=	Fall velocity of particles
K	=	Von Karman coefficient
g	=	Acceleration due to gravity
s	=	Water surface slope

Thus, for proper simulation of the distribution of sediment on a vertical, 'Z' in model should be equal to 'Z' in prototype for corresponding diameter of the sediment.

$$Z_m = \frac{w_m}{K_m \sqrt{g_m d_m s_m}} = Z_p = \frac{w_p}{K_p \sqrt{g_p d_p s_p}}$$

$$\therefore w_p = w_m \frac{K_p}{K_m} \sqrt{\frac{g_p d_p s_p}{g_m d_m s_m}}$$

$$\frac{K_p}{K_m} \text{ and } \frac{g_p}{g_m} \text{ are equal to 1}$$

Moreover in geometrically similar scale model

$$\frac{s_p}{s_m} = 1$$

Hence for geometrically similar scale models

$$w_p = w_m \sqrt{\frac{d_p}{d_m}} \quad (6)$$

Thus, a relationship between the diameter of low specific gravity material used in the model and that of the sediment in prototype can be worked out using above equation (CWPRS 2005). Value of K is 0.4 for clear water and reduces with sediment concentration. Sediment distribution equation given by Rouse, though qualitatively correct, has certain limitations. One of the most important limitations is that the theoretical exponent does not agree with the actual exponent. Secondly, it gives only the relative concentration distribution and the concentration at any level can be found only if Ca is known. Further, equation is satisfactory, even qualitatively, only in the main flow and not close to the bed. According to this equation, concentration at the water surface is zero and concentration at the bed is infinity. This is not true in practice; physical reasoning will show that the concentration at the bed should be finite. However, equation is valuable in as much as it provides a tool for studying the distribution of suspended load.

In earlier studies, a procedure of crushing the low specific gravity material and sieving the same through different sieves and remixing it in the required proportion for obtaining the desired size distribution curve or proportion of coarse, medium and fine fractions of the sediment in the prototype was adopted. This procedure was tedious and clumsy. To avoid these difficulties, the following alternative procedure was followed in the subsequent studies.

The available low specific gravity powder is analyzed for the determination of the size distribution curve. After injecting the material in the model, the settling efficiency of the chamber is determined by measurement of the volumes trapped at the outlet of the desilting chamber and flushing system, taking into due consideration of the volume of the sediment trapped inside the desilting chamber or by simultaneous measurements of the concentration in the inlet and both the outlets, the settling efficiency in the model is estimated. The expected settling efficiency using Camp's and others criteria is also

estimated, for the gradation curve using the mean diameter of the different fractions of the gradation curve and by integrating the results. Thus, once the satisfactory correlation between the model results and the estimated settling efficiency for the model parameters is established, the actual efficiency curve for sediment in the prototype could be estimated. This results not only convenience for the model studies but also enables to estimate the actual efficiency for the different gradation curves at site.

7. METHODOLOGY OF PHYSICAL MODEL STUDIES

Generally, suspended sediment is removed from desilting chambers by continuous flushing through silt flushing tunnel provided below. An extra discharge equal to about 20 % of design discharge is drawn through power intake for continuous flushing of settled sediment to maintain the desired settling efficiency. The layout and size of the flushing tunnels are so worked out that flushing velocity is maintained and total discharge did not exceed 20% of the design discharge. To achieve this objective one unit of desilting chamber is fabricated (out of multiple units) in fibre reinforced plastic (FRP) with transparent Perspex windows along with inlet transition, outlet transition and flushing tunnel below desilting chamber. Geometrically similar scale model is tested for settling efficiency and flushing efficacy for sediment removal by injecting crushed and sieved walnut shell powder material having low specific gravity.

The theoretical design of desilting chamber is tested for its optimum functioning in terms of its minimum length for maximum / designed settling efficiency and flushing efficacy along with the performance of inlet transition, openings connecting desilting chamber with silt flushing tunnel, settling trench, side slope of hoppers and outlet transition. During the experiments, a known quantity of low specific gravity material is injected at the inlet corresponding to designed sediment concentration. The model is run for about one day equivalent of prototype operation and settled sediment is recollected and measured at the downstream to calculate the experimental overall settling efficiency. This is compared with the analytical settling efficiency of the same material used in the model experiments. Further analysis is done to find out the settling efficiency for particle size of 0.2 mm and above. During the experiments, the inlet water level is maintained between MDDL and FRL. Design discharge is maintained at inlet, head race tunnel and silt flushing tunnel discharges are maintained at the outlet separately. During the experiments, if the performance of various parts of desilting chamber viz. inlet transition, outlet transition, settling trench etc. is not satisfactory, the modifications are done in consultation with project authorities and concerned model part is re-fabricated and tested to evolve optimum design.

For design parameters, the scope of reduction of length of desilting chamber is especially worked out,

which saves a huge amount of project cost as these are costly structures.

8. MATHEMATICAL MODELS

As far as the mathematical model studies for desilting chambers are concerned, various assumptions, approximations and simplifications are required to be made to make it convenient for numerical computations. Therefore, mathematical models are unable to provide required information on account of simulation and injection rate of suspended particles, inlet divergence (diffuser), opening sizes from desilting chamber to flushing tunnel for flushing sediments and dune formation in the hopper. Two and three dimensional flow patterns and the associated changes till now can be studied, only by using physical models because geometrical approximations can be considered adequately. After the development of numerical methods for simulation of two dimensional flow patterns, better mathematical models such as Computational Fluid Dynamics (CFD) software are available which may be tried for 3 D numerical model studies for the desilting chamber.

In the settling chamber flow is three dimensional especially in the inlet divergence and outlet convergence. At the inlet, there are structural arrangements for proper distribution of flow. Similarly, at the outlet the arrangements are made for smooth skimming off the flow layers containing less sediment in the suspension. Geometrical approximations are required to be made in two dimensional mathematical modeling which is not considered adequately in the mathematical modeling. All these add to the three dimensionality of the flow. The limitation of mathematical models is their ability to represent only two dimensional flows whereas; the flow in the prototype is three dimensional which is being nowadays taken care of by CFD.

Mathematical modeling through CFD

Computational Fluid Dynamics (CFD) is the computer solution of the governing equations for fluid flows (the conservation of mass, momentum, and energy) for three dimensions. Using CFD software is in many ways similar to setting up a physical experiment. If in a physical model, experiment is not set up correctly to simulate a real-life situation, then the results will not reflect the real-life solution, similar is the case for numerical model. It is important to ensure that the problem being modeled represents the actual physical situation as closely as possible. Simple hand calculations (Bernoulli's equation, energy balance, wave speed propagation, boundary layer growth, etc.) help in selecting physics and parameters, and provide checks to compare with results.

To conduct CFD model studies, the first step is to make exact 3 D geometry of the desilting chamber. Then mesh is created to define the flow area, inlet and outlet boundary conditions are specified and model is run for simulation. Initially, desilting chamber model studies may be done using the CFD program before conducting physical model studies as it is comparatively difficult to make additions and alterations in a physical model. Various design parameters such as length of desilting chamber, length and bed slope of inlet transition, outlet transition, size and spacing of openings connecting main chamber with silt flushing tunnel etc. may be tested on this CFD program and only the best possible alternative may be selected to conduct physical model studies to finalized the design.

Thus, CFD can be used as a complementary tool for analysis of flow in desilting chambers.

9. LIMITATIONS OF MODEL STUDIES

It does not necessarily follow that model studies provide ready answers to all questions. For, one cannot devise a suitable model test or interpret the model test results, unless one understands the basic theory of the phenomenon under study. Time and money are wasted by a test of a model that does not adequately represent the prototype. Sometimes it is impractical to build a model that will furnish all the desired information. And lastly, it is wasteful to resort to model study if the results can be predicted by theory. In spite of these limitations, model tests have proved to be invaluable in many cases and the use of models in hydraulic engineering is steadily increasing. However, following are the limitations for desilting chamber models.

- In case of hydraulic model experimentation, it is the hydraulic similitude and not geometric similitude, which is the guiding and controlling factor in the design of models. Hydraulic similitude is ensured by satisfying Froude's law.
- Quantitative estimation of the performance of flushing system could not be attempted since low specific gravity material based on weight-volume relationship of the sediment in the model differed from the prototype.
- Efficiency of desilting chamber in prototype is expected to be more than that estimated using the model results, as the ratio of size of opening to the size of particle to be removed is very high in prototype than that in the model.

- In Nature, the forces that play, cannot be gauged accurately, neither the duration of forces for which the resultant action is responsible is known. It is therefore, to be found out from actual experiments, the optimum hour that a particular model should be run so as to be able to faithfully represent the prototype conditions. It is only possible for a skilled observer with long practical experience to diagnose from the performance of a model, how far the results can be relied on and to what extent they can be applied in practice.

It is difficult to simulate all the conditions and properties of nature in the hydraulic models and consequently difficulties do arise in the translation of results obtained from studies in the models. The hydraulic models have, therefore, been considered as means towards an end in predicting certain factors at least qualitatively to be met within the prototype (Verma 2002).

10. FIELD DATA REQUIRED FOR CONDUCTING MODEL STUDIES

Following field data are required for conducting hydraulic model studies for desilting chambers:

- (i) Preliminary drawing of the desilting chambers viz. longitudinal section, plan, cross-sections at important locations along with design calculations.
- (ii) Flushing arrangement drawing along with design calculations.
- (iii) Concentration of the suspended sediment giving breakup of coarse, medium and fine sediment.
- (iv) Gradation curves of bed material and suspended sediments.
- (v) Maximum sediment concentration for which studies are to be conducted.
- (vi) Details of inlet and outlet transitions of the chambers.
- (vii) Discharge of each unit of desilting chamber at inlet and outlet.
- (viii) Size of openings in trash rack.

11. CONCLUSIONS

The design of desilting basin in each case has to be wisely determined considering the type of turbine and the base metal of underwater parts and sediment characteristics. There are several approaches for determining the size of a desilting chamber. These basically depend on size of particle to be excluded and its fall velocity. The approaches differ in accounting for the effect of turbulence and concentration of sediment on fall velocity of particle. These approaches are found to give largely varying size of chamber for a particular size of sediment to be excluded. Hydraulic model studies are important because it

facilitates the visualization of flow, sediment movement and advantage of finalizing efficient inlet and outlet transition, size and spacing of holes connecting main chamber to silt flushing tunnel and silt flushing arrangement besides the determination of sediment removal efficiency. Especially, the scope of curtailment of length of main chamber is ascertained by the model studies. These are the basis for the necessity of a model study for design optimization of desilting chamber.

12. ACKNOWLEDGEMENT

The authors sincerely thank Shri S. Govindan, Director, CWPRS for constant encouragement, guidance and kind permission for publishing this paper. The authors are also thankful to various project authorities for referring studies to CWPRS and making available the necessary data for conducting the model studies.

References

- Acharekar, C.L. and Narain, P. (1978). A Rational approach to tackle silt erosion of hydro turbine components. Proc. Seminar held at WRDTC, IIT, Roorkee, India.*
- Asthana, B.N. (2007). Sediment Management in Water Resources Projects. CBI&P, New Delhi, Pub. No. 301.*
- CBIP (1954). Role of models in the evaluation of hydraulic structures. Pub. No. 53.*
- CWPRS (2005). Guidelines for design of desilting basins (Pressure flow). Technical Memorandum.*
- Du-Tong (1981). Cavitation and wear on hydraulic machines. Journal of Water Power and Dam Construction.*
- Mosonyi, E. (1965). Water Power Development – II. Publishing House of the Hungarian Academy of Sciences, Budapest.*
- Qamar, M.Z., Verma, M.K., Bhosekar, V.V. and Meshram, A.P. (2014). Critical review of various approaches for settling efficiency of desilting basins. CBIP - Conference on Challenges and Barriers in Hydropower Development, Shimla on 18-19 Sept 2014.*
- Rouse, H. (1949). Engineering Hydraulics. John Wiley & Sons Inc. New York.*
- Verma, M.K. (2002). Analysis of model studies for desilting basins. M. Tech Dissertation, WRDTC, IIT, Roorkee, India*

Numerical Computation for Sizing of Break Pressure Tanks

N.N. Sontake¹, A.D. Vasudeo², A.D. Ghare³, R.N. Ingle⁴

¹Research Scholar, Department of Civil Engineering, VNIT, Nagpur - 440010, India

²Assistant Professor, Department of Civil Engineering, VNIT, Nagpur - 440010, India

³Associate Professor, Department of Civil Engineering, VNIT, Nagpur - 440010, India

⁴Professor(Retd.), Department of Civil Engineering, VNIT, Nagpur - 440010, India

Email: nitinsontake@gmail.co.in , avasudeo@yahoo.com , adghare@yahoo.co.in,
rningle@gmail.com Telephone/Mobile No.: +91 9960594529, 9096475353

ABSTRACT

For transporting a large quantity of water from a source to desired location at a long distance, large sized pipes are used. Water can be transported by gravity or by pumping. In most of the cases, water is transported by pumping. For economic consideration, these pipelines are laid following the ground level profile. In some situations, the longitudinal profile of the pipeline may be highly undulating. Pipelines laid, following an undulating nature of the ground, usually create an inverted siphon type of pipeline profile. Installation of Break Pressure tanks (BPT) at proper locations on such pipelines can provide a good solution to control water hammer pressure in the pipeline within desirable limits. In this paper, a pipeline on the downstream side of the BPT is forming a shape of an inverted siphon, has been analyzed to obtain the appropriate size of the BPT. Based on the analysis of unsteady flow in the pipeline, mathematical expressions have been derived to express the relationship between the area of the BPT provided and the maximum level to which the water in the BPT would rise. The governing equations are nonlinear in nature and as such, to obtain a general solution of these equations, an approximation has been introduced by replacing the velocity variable. A case study has been presented to compare the applicability of approximate linearized differential equations with nonlinear differential equations by solving the governing nonlinear differential equations using MATLAB.

Keywords: - Pumping Main, Unsteady Flow, Numerical Simulation, Break Pressure Tanks

1. INTRODUCTION

Conveyance of water from a source to the water treatment plant is generally carried out by the long and large diameter pipelines. These pipelines are generally laid following a ground level profiles. If inlet and outlet elevation difference is large, such pipelines undergo variation in pressure during valve operations (Jordon 1984). Variation in pressure is responsible for the water hammer effect and can rupture the pipeline (Kirmeyar et al. 2001). To avoid possible effect of water hammer pressure various pressure reducing devices are used. Flywheel, air chamber, surge tank and air valves are few among them. Break Pressure Tank (BPT) is an open tank, operates under atmospheric pressure and generally installed in the

long and large diameter pipeline to avoid the water hammer pressure. Functioning of the BPT depends upon its location on the pipelines and are generally provided on high summit points. BPT allows the flow to discharge into the atmosphere, thereby reducing its hydraulic pressure to zero or atmospheric pressure (Johnson 1977, Jordon 1984, Niskanen 2003).

Importance of providing BPT on the pipeline and its stability against earthquake forces (Blackwell, 1979), feasibility aspect of the BPT (McNAbola et al. 2011), are available in the present literature. However, no attempt has been made to determine the size of the BPT. The method currently used for evaluating the BPT's size is based on the detention period; this method gives the volume of the BPT. On the basis of the volume of the tank, cross sectional area and height of the BPT cannot be determined. In practical situation, based on the volume; height and the area of the BPT is arbitrarily decided. This arbitrary dimensioning of the BPT yields larger or smaller size of the BPT. It is important to highlight that, if the size of the BPT is large enough, it remains empty during the operations of the pipelines; whereas, if the size of the BPT is small, it overflows (Ager et. al 2011).

In some cases, depending on the BPT – pipeline geometry and flow characteristics, and specifically during the BPT filling, the water level into the BPT undergoes oscillations which can be greater than water level under steady state conditions. If BPT is designed under the steady flow condition rather than under unsteady flow conditions, the water overflows out of the BPT. Therefore, a more rational approach is essential for dimensioning of the BPT. In this paper, a pipeline on the downstream side of the BPT is forming a shape of an inverted siphon, has been analyzed to obtain the appropriate size of the BPT. Based on the analysis of unsteady flow in the pipeline, mathematical expressions have been derived to express the relationship between the area of the BPT provided and the maximum level to which the water in the BPT would rise.

2. MECHANISM OF BPT – PIPELINE SYSTEM

Filling process of the BPT, located at a high summit point between the pumping main and a water treatment plant is mainly governed by the pipeline profile on the downstream side of the BPT. The pipeline laid following the ground level profile may either be plain, undulating or slopping. When the nature of the ground is continuously sloping, due to gravity effect, BPT – pipeline will remains empty after stopping the inflow to the system. When inflow starts filling the empty BPT and the pipeline, water level in the BPT starts rising gradually till the velocity in the pipeline attain a steady state condition. Rise in a water level in the BPT corresponding to a steady state velocity in the pipeline will be the maximum rise in water level in the BPT. In such case the height of the BPT will be equal to the maximum frictional

losses for the particular pipe at a steady state velocity. When topography or elevation of the ground changes abruptly, the pipeline is laid following such profile will be in the form of an inverted siphon (Fig.1). During no operation condition water remains in the pipeline up to the level of the outlet of BPT in stagnant condition. During operation of the pipeline, if the size of BPT is not adequate, there will be overflow as the rate of rise of water level will not become zero when it reaches the steady state value.

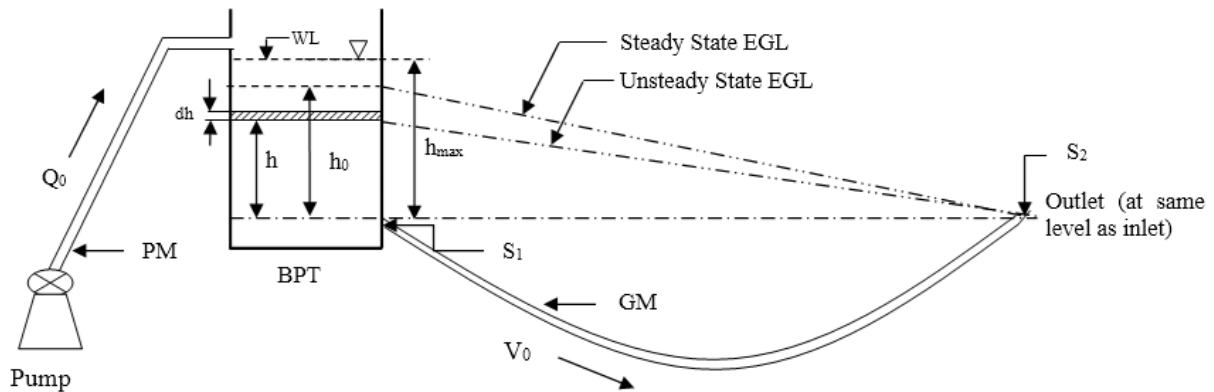


Figure 1 Inverted siphon type BPT - pipeline profile

3. ANALYSIS OF UNSTEADY FLOW IN THE PIPELINE PROVIDED WITH BPT

Equations describing the unsteady flow in the pipeline system have been derived from the first principle of conservation of mass and conservation of momentum. As shown in Fig (1), when the steady state discharge from the pump starts filling the BPT, the velocity (V) changes continuously from 0 to V_0 (steady state velocity) and the quantity of water ($Q_0 - A_p V$) raises the water level in the BPT or develops head. This developed head pushes the stagnant water in the inverted siphon portion of the pipeline.

Thus, Inflow – Outflow = Change in control volume per unit time

$$Q_0 - A_p \cdot V = A_{BPT} \cdot \frac{dh}{dt} \quad (1)$$

where: Q_0 = constant inflow discharge; A_p = cross sectional area of the pipe; V = velocity of flow in the pipe under unsteady flow conditions; A_{BPT} = cross sectional area of the BPT; h = total head at the inlet; and t = time

The Bernoulli equation applied between the section at the pipeline inlet and the section at the pipeline outlet (see Fig. 1) under unsteady flow conditions is given by the following equation:

$$z_1 + \frac{p_1}{w} + \frac{V_1^2}{2g} = z_2 + \frac{p_2}{w} + \frac{V_2^2}{2g} + \sum h_l + h_f + h_a \quad (2)$$

where: z_1 and z_2 = elevation at the pipe inlet and outlet, respectively; p_1/w and p_2/w = pressure head at the pipe inlet and outlet, respectively; $V_1^2/2g$ and $V_2^2/2g$ = velocity head at the pipe inlet and outlet, respectively; $\sum h_l = \sum K (V^2/2g)$ = sum of the local head losses in the reach between sections 1 and 2; $\sum K$ = sum of the local loss coefficients in the reach between sections 1 and 2; $h_f = f L/D (V^2/2g)$ = friction head loss; f = friction factor; L = pipe length; D = internal pipe diameter; $h_a = L/g (dV/dt)$ = acceleration head; w = specific weight; and g = acceleration due to gravity.

By rearranging Eq. (2), it can be re-written as follows:

$$h = F \cdot V^2 + \frac{L}{g} \cdot \frac{dv}{dt} \quad (3)$$

where:

h = difference between the total head loss at entrance and the total head loss at exit;

$$F = \left(\sum K + 1 + f \cdot \frac{L}{D} \right) \cdot \frac{1}{2g} = \text{coefficient in the friction loss formula}$$

Eqs. (1) and (3) govern the flow in the pipeline from BPT to outlet. To obtain the expressions for V and h in terms of time, these equations have been solved with the boundary condition, at $t = 0$, $V = 0$ and $h = 0$ and at steady state $t = \infty$, $V = V_0$ and $h = h_0$. Differentiating equation (3) with respect to t and substituting the value of $\frac{dh}{dt}$ in equation (1) and rearranging the terms,

$$\frac{d^2V}{dt^2} + \frac{2FVg}{L} \frac{dv}{dt} + \frac{g A_p}{A_{BPT}} \cdot V = \frac{Q_0 g}{A_{BPT} L} \quad (4)$$

Eq. (4) is a second order nonlinear differential equation in the form of variable, V and its general solution is not possible. As V is a basic parameter for establishing the criterion for sizing of the BPT, it is necessary to linearize the Eq. (4), or obtain a solution of Eq. (4) by using numerical methods.

3.1 Solution based on linearized equations

To obtain a general solution for Eq. (4), an approximation has been introduced by replacing the variable V in the coefficient of dV/dt in the second term of Eq. (4) by its average value as, $\frac{1}{2}V_0$. With this assumption, Eq. (4) can be written as,

$$\frac{d^2V}{dt^2} + \frac{2FV_0 g}{L} \cdot \frac{dv}{dt} + \frac{g A_p}{A_{BPT}} \cdot V = \frac{Q_0 g}{A_{BPT} L} \quad (5)$$

$$\frac{d^2V}{dt^2} + \frac{2FV_0g}{L} \cdot \frac{dv}{dt} + \frac{gA_p}{A_{BPT}} \cdot V = \frac{Q_0g}{A_{BPT}L} \quad (5)$$

or;

$$\frac{d^2V}{dt^2} + b_1 \cdot \frac{dV}{dt} + b_2 \cdot V = b_3 \quad (6)$$

where:

$$b_1 = \frac{FgV_0}{L}$$

$$b_2 = \frac{gA_p}{A_{BPT}L}$$

$$b_3 = \frac{Q_0g}{A_{BPT}L}$$

From the substitution made for b_1 and b_2 the cross sectional area of the BPT can be obtained. This area is actual required area of the BPT and is given by,

$$A_{BPT} = \frac{4A_pL}{F^2V_0^2g} \quad (7)$$

Eq. (6) being linear in nature, its general solution can be obtained. This solution can be used to calculate the velocity and as such the rise in the water level in BPT. Solution of Eq. (6) develops two cases. In first case b_1^2 will be greater than or equal to $4b_2$ and in second case b_1^2 will be less than $4b_2$. When $b_1^2 \geq 4b_2$ the velocity in the pipeline approaches the steady state value (V_0) asymptotically and hence rise in water level in the BPT which is dependent on velocity will also attain the steady state condition asymptotically. Therefore, if the criterion given in first condition ($b_1^2 \geq 4b_2$) satisfied for the cross sectional area of the BPT then water level in the BPT will never rise above its steady state value. Solution to case two give oscillatory behavior of velocity. In this paper only first case has been discussed.

Horizontal (Value) Axis

The auxiliary equation corresponding to Eq. (6) is,

$$n^2 + b_1n + b_2 = 0 \quad (8)$$

roots of an auxiliary equation can be written as,

$$n = \frac{-b_1}{2} \pm \frac{1}{2} \sqrt{b_1^2 - 4b_2} \quad (9)$$

When $b_1^2 \geq 4b_2$, the variation in rise velocity in the BPT can be obtained by general solution of Eq. (6) and can be expressed as,

$$V_1 = C_1e^{n_1t} + C_2e^{n_2t} + V_0 \quad (10)$$

By performing appropriate mathematical steps the variation of rise in water level in BPT is obtained as,

$$h_1 = \left[\frac{L}{g} \cdot C_1 \cdot (n_1 \cdot e^{n_1 t}) + C_2 \cdot (n_2 \cdot e^{n_2 t}) \right] + F \cdot [C_1 \cdot e^{n_1 t} + C_2 \cdot e^{n_2 t} + V_0]^2 \quad (11)$$

where:

$$C_1 = V_0 \cdot n_2 \cdot \left(\frac{1}{n_1 - n_2} \right) = \text{constant of integration}$$

$$C_2 = V_0 \cdot n_1 \cdot \left(\frac{1}{n_2 - n_1} \right) = \text{constant of integration}$$

n_1 and n_2 = roots of auxiliary equation

3.2 Solution based on numerical method

To obtain a general solution for Eq. (6) an approximation has been introduced by considering the average value of velocity. With this approximation values obtained for the variation in velocity and head in the BPT may differ than actual values, therefore to check the possible deviations, Eq. (5) has been solved by using ODE–45 solver of MATLAB.

4. CASE STUDY

To validate the output of the developed mathematical expressions, experimental case scenario was generated in the laboratory. The results of the case have been compared. An experimental set up was fabricated at the Hydraulics and Fluid Mechanics Laboratory, Department of Civil Engineering, Visvesvaraya National Institute of Technology, Nagpur, India (Fig. 2). The experimental setup is self contained type, having circulating arrangement. Downstream side of the BPT act as rising main. It consists of water sump of 1000 liters capacity for a continuous supply of water. To lift the water and maintaining a flow range of 0.0009 to 0.0019 m^3/s , a rigid PVC pipe with an internal diameter of 0.0508 m , attached with 2 HP low head high discharge pump was used. The outlet of the pump was connected to a delivery pipe via gate valve to vary the discharge to the BPT. The delivery pipe was finally taken to BPT. A measuring scale was attached with the BPT to measure the rise in water level in BPT. An outlet arrangement was made in the BPT to connect flexible PVC pipe of 21 m length and 0.0508 m internal diameter forming the shape of inverted siphon. The BPT has a cross sectional area of 0.0637 m^2 and a height of 1.2 m . The outlet of flexible PVC pipe and the bottom of BPT was kept at the same level. The final discharge through an inverted siphon type pipeline profile was collected in a collection tank (1 × 1 × 0.750 m) attached with measuring scale to measure the discharge by volume.

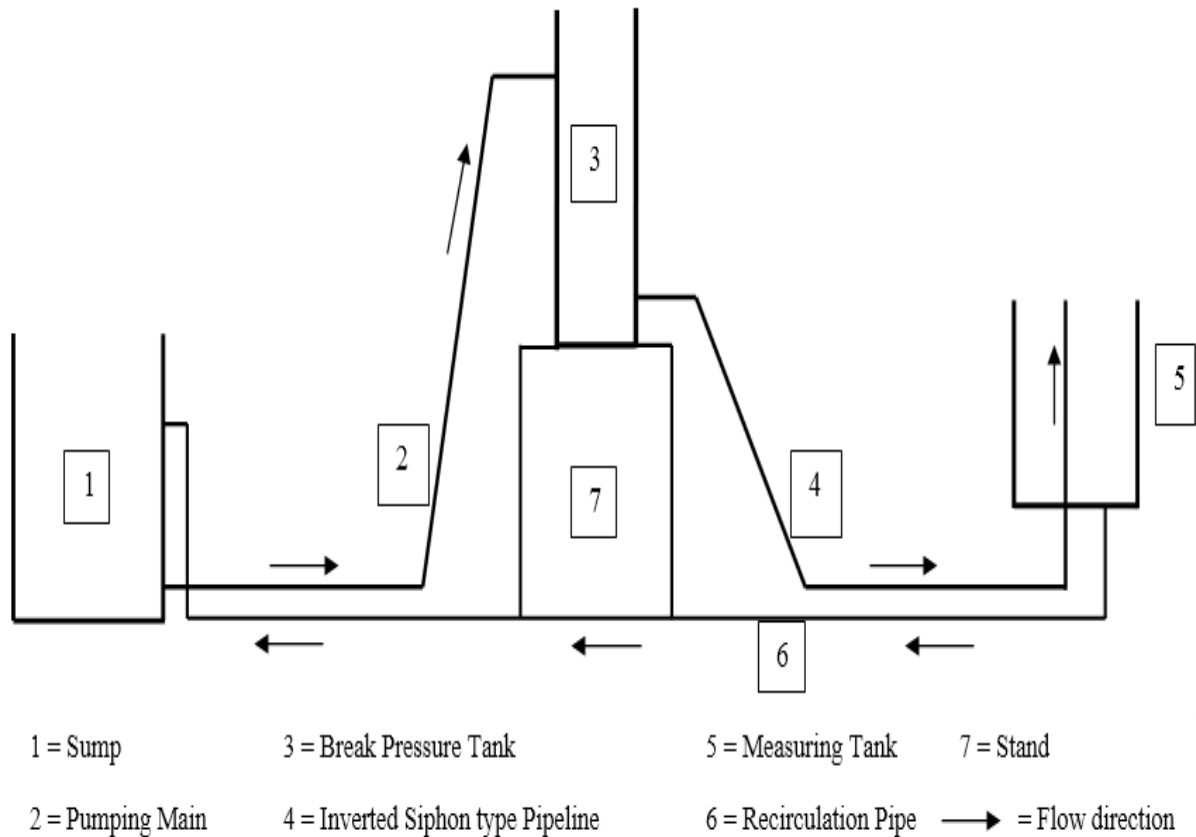


Figure 2 Schematic line diagram of experimental setup

5. EXPERIMENTAL OBSERVATIONS

The pump was started to commence the flow, this flow was regulated through the operation of gate valve fixed to the pipeline to achieve the desired range of the discharge. The rise of water level in BPT has been continuously observed and the maximum value of water level (h_{Max}) is recorded. For this discharge, the flow condition in the pipeline is allowed to reach its steady state. The steady state value of water level in the BPT (h_0) which is same as the h_{Max} is recorded. Discharge (Q_0) corresponding to each observation is measured by volumetric method. The procedure was repeated for number of observations.

5.1 Comparison of experimental observations with analytically and numerically calculated values

Corresponding to all the experimental values of V_0 the maximum rise in water level in the BPT are observed, these values are called as h_{Maxobs} and are shown in Table 1. Values of h_{Max} as a function of time are calculated by using Eq. (11). These values are called as $h_{Maxcalc}$ and are shown in Table 2 and Fig. 3.

Table 1 Table showing the observed values of maximum rise in water level in BPT

<i>Obs No.</i>	$h_{Max\ obs} (m)$	$Q_0 (m^3/s)$	$V_0 (m/s)$	F
1	0.279	0.000984	0.485388	1.133236
2	0.28	0.001001	0.49396	1.096591
3	0.38	0.001172	0.578201	1.08568
4	0.408	0.001256	0.619844	1.01096
5	0.477	0.001346	0.663987	1.030961
6	0.534	0.001413	0.697083	1.047967
7	0.577	0.001512	0.745879	0.986176
8	0.582	0.001527	0.753413	0.974345
9	0.634	0.001631	0.804905	0.927619
10	0.681	0.001643	0.810738	0.985094
11	0.721	0.001699	0.838066	0.975578
12	0.823	0.001751	0.863953	1.051637
13	0.86	0.00189	0.932349	0.938363
14	0.93	0.001928	0.951376	0.976523

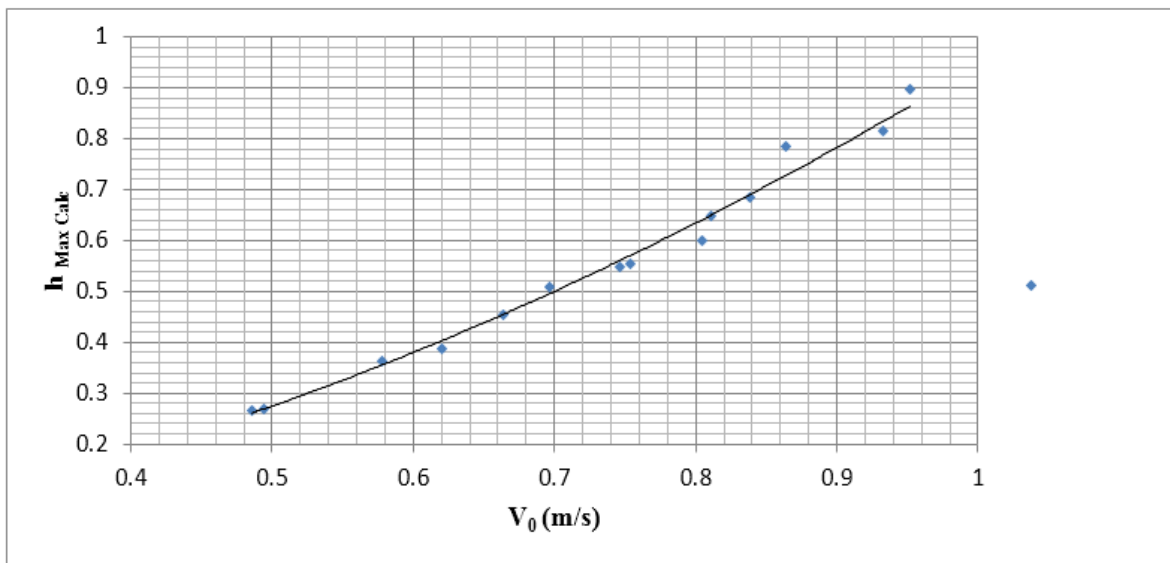


Figure 3 Variation of $h_{Max\ calc}$ (using Eq.11) with V_0

Assuming that the experimentally observed values are correct, these are compared with analytically calculated values and percentage deviation in results for each observed values is calculated. These values are shown in Table 2. It is important to note that all the observed values of $h_{Max\ obs}$ are higher than all corresponding analytically calculated values of $h_{Max\ calc}$. the difference being, of the order of 4% to 6%, which may be because of the primary assumption made for linearizing the Eq. (5), in addition to presence of fully rigid boundary and incompressibility of the fluid.

Table 2 Percentage deviation between the experimentally observed and analytically calculated (Eq.11) values of h_{Max}

Obs No.	$h_{Max\ obs} (m)$	$h_{Max\ calc} (m)$	Deviation (%)
1	0.279	0.266	4.49
2	0.280	0.267	4.64
3	0.380	0.362	4.69
4	0.408	0.388	5.04
5	0.477	0.454	4.94
6	0.534	0.509	4.86
7	0.577	0.548	5.16
8	0.582	0.553	5.23
9	0.634	0.600	5.49
10	0.681	0.647	5.17
11	0.721	0.685	5.22
12	0.823	0.784	4.86
13	0.860	0.815	5.44
14	0.930	0.896	3.73

The variation in rise in velocity with time for each observed values of V_0 is calculated by coding a program in MATLAB. These variations in velocity are shown in Fig. 4. Also, the variation in rise in water level with time for each observed values of V_0 is calculated by coding a program in MATLAB. These variations in rise in water level are shown in Fig. 5. From the curves of Fig. 5, maximum values are obtained for each set of observation and represented as h_{MaxNum} in Table 3. The variation in h_{MaxNum} with V_0 is shown in Fig 6. Assuming that the experimentally observed values are correct, these are compared with numerically calculated values. Percentage deviation in results for each observed values is calculated and shown in Table 3. In this case also, h_{MaxObs} values are 4% to 6% higher than all the corresponding values of h_{MaxNum} .

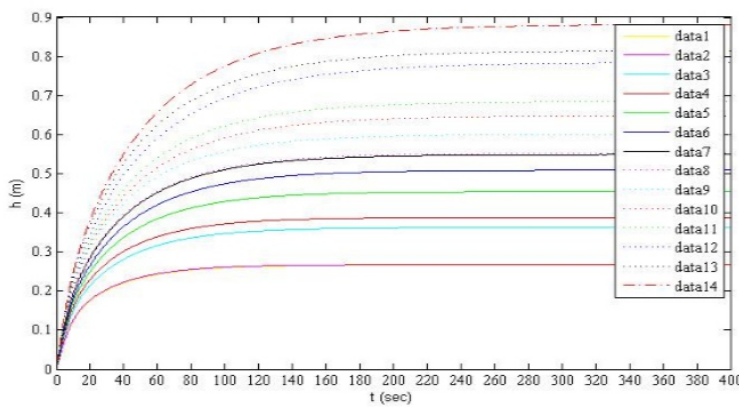


Figure 4 Variation of estimated rise in water level using MATLAB in the BPT with respect to time

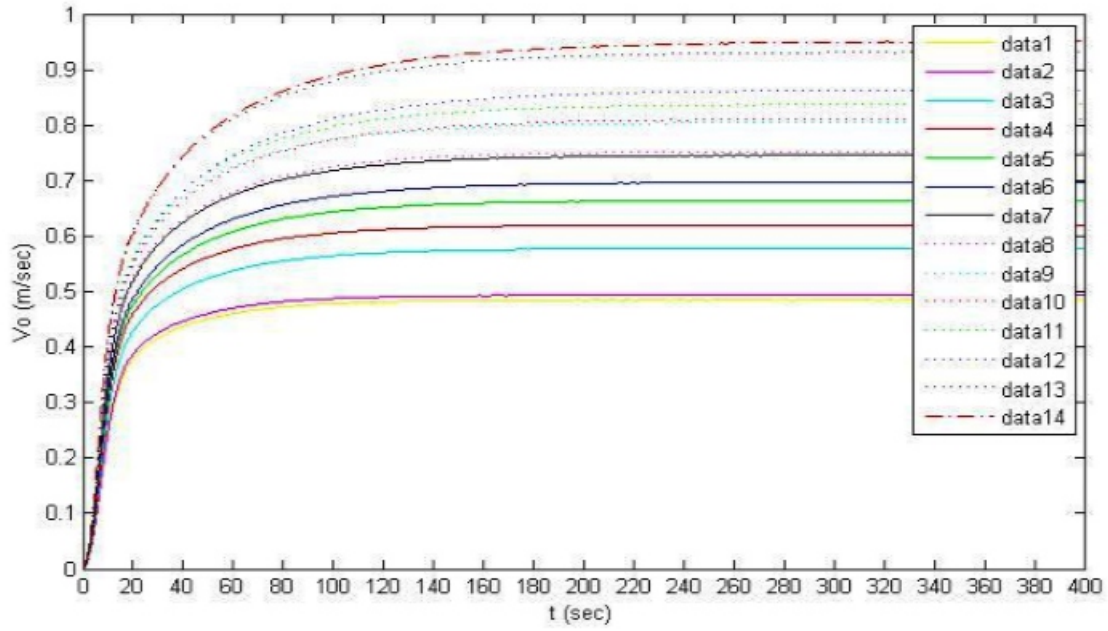


Figure 5 Variation of estimated rise in velocity using MATLAB in the BPT with respect to time

Table 3 Percentage deviation between the experimentally observed and numerically calculated (MATLAB) values of h_{Max}

<i>Obs No.</i>	$h_{Max\ obs} (m)$	$h_{Max\ Num} (m)$	<i>Deviation (%)</i>
1	0.279	0.266	4.69
2	0.280	0.267	4.67
3	0.380	0.362	4.82
4	0.408	0.388	5.07
5	0.477	0.454	4.92
6	0.534	0.509	4.89
7	0.577	0.548	5.13
8	0.582	0.552	5.37
9	0.634	0.600	5.54
10	0.681	0.647	5.10
11	0.721	0.684	5.30
12	0.823	0.784	4.89
13	0.860	0.814	5.54
14	0.930	0.882	5.35

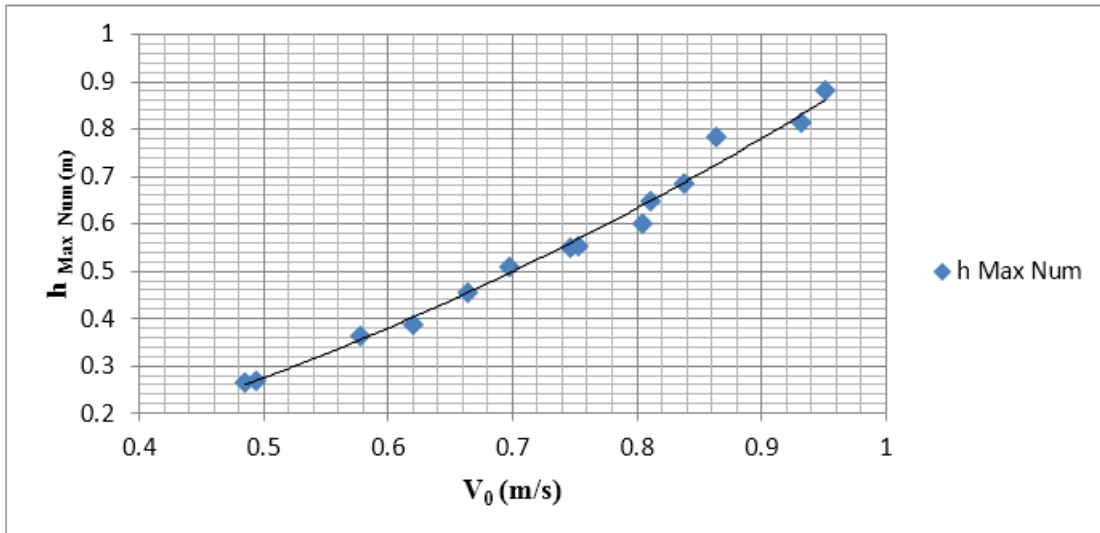


Figure 6 Variation of $h_{Max Num}$ (using MATLAB) with V_0

Comparison between the rise in water level in the BPT, calculated by analytical and numerical methods with the experimentally observed values is shown in Fig. 7. Since all the observed values are higher than $h_{Max calc}$ and $h_{Max Num}$, the BPT designed for height based on $h_{Max calc}$ and $h_{Max Num}$ with suitable free board of 500 mm to 1 m, will never overflow.

Calculations for $h_{Max calc}$ using Eq. (11) and $h_{Max Num}$ by coding program in MATLAB are very cumbersome, hence simplified regression equations has been proposed as an alternative for selecting the cross sectional area and the height of the BPT.

As determined by regression analysis, the equation for $h_{Max calc}$ (Fig.3) is,

$$h_{Max calc} = 0.943 \times V_0^{1.781} \quad (12)$$

with coefficient of determination, $R^2 = 0.991$

As determined by regression analysis, the equation for $h_{Max Num}$ (Fig.6) is,

$$h_{Max Num} = 0.940 \times V_0^{1.775} \quad (13)$$

with coefficient of determination, $R^2 = 0.992$

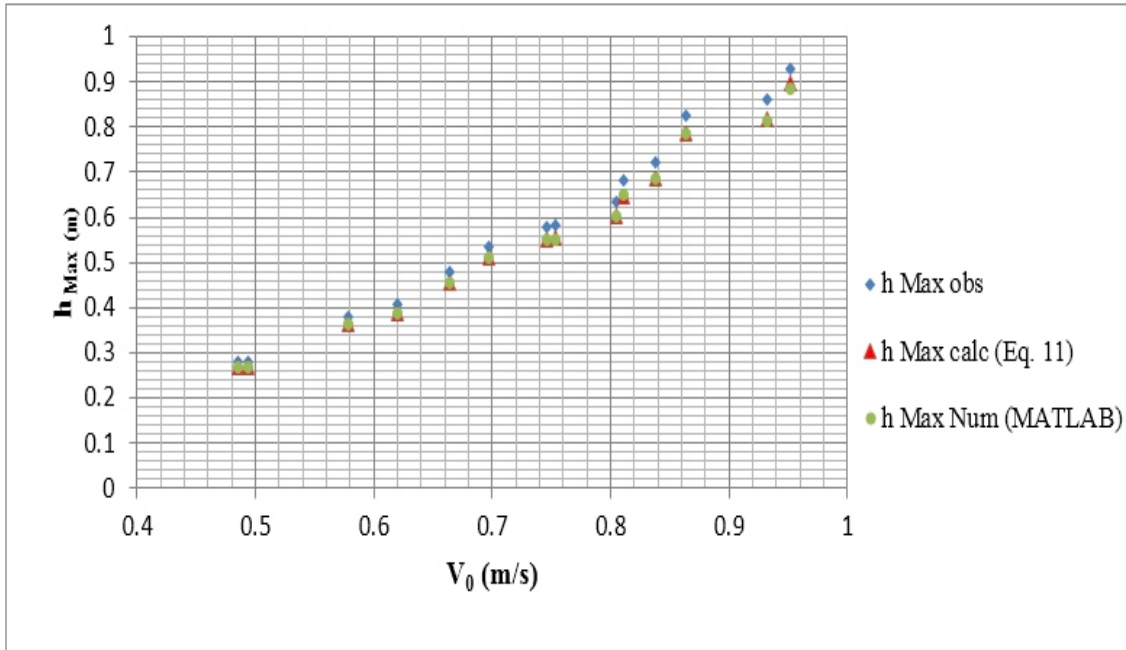


Figure 7 Comparison of analytical, numerical and experimental values of h_{Max}

6. CONCLUSIONS

In the research presented through this paper, a method based on transient flow analysis has been developed and proposed for selection of proper size of the BPT. Equations for variation in rise in velocity and water level in the BPT have been investigated. These equations have been validated experimentally and numerically. Based on this method, following conclusions are drawn,

1. When the longitudinal profile of pipeline downstream of BPT is uniformly sloping downwards, only a nominal sized BPT is sufficient and the height of BPT can be decided from the elevation of water level required to overcome frictional loss corresponding to steady state discharge.
2. When $b_1^2 \geq 4 b_2$, the required cross sectional area of the BPT can be obtained by Eq. (7). In this case, water level in the BPT during unsteady flow condition will never rise above the steady state water level.
3. Also when $b_1^2 \geq 4 b_2$, the maximum value to which the water level in the BPT will rise during unsteady flow conditions can be obtained by either Eq. (12) or Eq. (13); which are marginally different, as given below

$$h_{Max\ calc} = 0.943 \times V_0^{1.781} \quad (12)$$

$$h_{Max\ Num} = 0.940 \times V_0^{1.775} \quad (13)$$

7. NOTATIONS

The following symbols are used in this paper:

A_p = cross sectional area of the pipe;

A_{BPT} = cross sectional area provided for BPT;

BPT = break pressure tank;

b_1, b_2, b_3 = coefficients of the terms in the linearized differential equation for unsteady state;

D = internal pipe diameter;

data (1 to 14) = obs (1 to 14);

F = coefficient in the friction loss formula;

f = friction factor;

GM = gravity main;

g = acceleration due to gravity;

h = total head at the pipe entrance under unsteady flow conditions;

h_{Max} = maximum rise in water level in the BPT under unsteady flow conditions;

$h_{Maxcalc}$ = maximum calculated head at the pipe entrance under unsteady flow conditions;

h_{MaxNum} = numerically calculated maximum water level in the BPT;

h_{Maxobs} = maximum observed head at the pipe entrance under unsteady flow conditions;

h_0 = total head at the pipe entrance under steady flow conditions;

h_a = acceleration head;

h_f = friction head loss;

HGL = hydraulic gradient line;

L = pipe length;

n = roots of auxiliary equation;

Obs = observations;

PM = pumping main;

Q_0 = constant inflow discharge;

S_1 = section – 1 at the outlet of the BPT;

S_2 = section – 2 at the outlet of the pipeline;

t = time;

V = flow velocity in the pipe under unsteady flow conditions;

V_0 = flow velocity in the pipe under steady flow conditions;

w = specific weight of fluid;

WL = water level in the BPT;

C_1 and C_2 = constants of integration;

z_1 and z_2 = elevations at the pipe inlet and outlet respectively;

Σh_f = total head loss in the pipeline;

ΣK = sum of the local loss coefficient in the reach between section 1 and 2;

$\frac{P_1}{w}$ and $\frac{P_2}{w}$ = pressure heads at the pipe inlet and outlet respectively;

$\frac{V_1^2}{2g}$ and $\frac{V_2^2}{2g}$ = velocity heads at the pipe inlet and outlet respectively;

8. REFERENCES

- Blackwell, F. N. (1979). "A Study of the Earthquake Resistance of Domestic Break Pressure Tanks". *Bulletin of the New Zealand National Society for Earthquake Engineering.*, 12 (3), 168-173.
- Dak, S. K., Saxena, P., Pandey, S. N., Kedarpawar, M. N., Malhotra, J., and Gupta, N. (1990). "Study of Break Pressure Tank – Pipe System". A thesis submitted in partial fulfillment of the requirement for the degree of Bachelor of Engineering, in Civil Engineering, Visvesvaraya Regional College of Engineering, Nagpur, India., 36 – 37.
- Brown, L. (2006). "Understanding Gravity-Flow Pipelines Water Flow, Air Locks and Siphons". *Livestock, Watering Factsheet, British Columbia, Ministry of Agriculture and Lands, Order No. 590.304-5.*
- Johnson, C. R. (1977). "Standards and Procedures for the Design of Water Supply Systems in Rural Areas of Nepal and Bhutan". University Press, Tribhuvan University, Kathmandu, Nepal.
- Jordon, T. D. Jr. (1984). "Handbook of Gravity-Flow Water System for Small Communities". A reference manual for surveying, designing, and constructing gravity flow water system, government of Nepal.
- Kirmeyer, G. J., Friedman, M., Martel, K., Howie, D., LeChevallier, M., Abbaszadegan, M., Karim, M., Funk, J., and Harbour, J. (2001). "Pathogen Intrusion into the Distribution System". AWWA Research Foundation and the American Water Works Association, Denver, CO.
- McNobola, A. Coughlan, P. and Williams, A. P. (2011). "The Technical & Economic Feasibility of Energy Recovery in Water Supply Networks". *Renewable Energy and Power Quality Journal*, 9.
- Niskanen, Matthew A. (2003). "The Design, Construction, and Maintenance of a Gravity-Fed Water System in the Dominican Republic". M.Sc. Thesis, Department of Civil Engineering, Michigan Technological University.
- Tim Ager, Aasiyah Baig, Paul Bireta, Patrick Dunlap, Elliott Gall, Stephen Mathai, Hannah Romaine, David Rounce, Fernando Salas, James Seppi, Daniel Siegel and Corrie Thompson. (2011). "Alternative Analysis Report, Water & Health Project". Greater Austin, Panama, Engineers without Borders, document 523, USA, 28-29.

Curve Number Derivation For Experimental Plots Of Different Slopes, Hydrologic Soil Groups And Land Use

Mohan Lal^{1*}, Surendra Kumar Mishra², Ashish Pandey³

¹Research Scholar, Department of Water Resources Development and Management, Indian Institute of Technology, Roorkee-247667, UK, India, Email: mohan841987@gmail.com, Mobile No.: +91-8439899375 (*Corresponding Author)

²Professor, Department of Water Resources Development and Management, Indian Institute of Technology, Roorkee-247667, UK, India.

³Associate Professor, Department of Water Resources Development and Management, Indian Institute of Technology, Roorkee-247667, UK, India.

ABSTRACT

The Soil Conservation Service-Curve Number (SCS-CN) method is one of the most popular methods for computing the volume of direct surface runoff for a given rainfall event. In this study, CN method is evaluated at plot scale using the data of a large number of observed rainfall (P)/runoff (Q) events for 21 agricultural experimental plots located in Roorkee, Haridwar, Uttarakhand, India. The derived CN values from observed P-Q (CN_{PQ}) data were considerably different from conventional NEH-4 table (CN_T) values. CN_T values derived from plot characteristics do not estimate the runoff from these plots as accurately as do the CN_{PQ} . For example, optimized CN for natural P-Q data series (CN_{LSN}) generally performed the best of all, and median curve number (CN_m) derived from P-Q data set generally better than CN_T . The optimized initial abstraction ratio (λ) values showed that the original assumption of the $\lambda = 0.20$ is unusually high. Most of the derived λ values (respectively 20 and 16 out of 21 for natural and ordered P-Q data sets) are less than the default $\lambda = 0.2$ value. The median and mean λ values were respectively 0 and 0.039 for natural P-Q data and 0.046 and 0.127 for ordered P-Q data. The initial abstraction (I_a) was not linearly proportional to the potential maximum retention (S). As expected, CN (or, potential maximum retention, S) values showed a higher degree of dependence on the physically observed 1-day antecedent soil moisture ($\theta_{o,1}$) than, 5-day average antecedent soil moisture ($\theta_{o,5}$), and 5-day antecedent rainfall (P_5).

Keywords: - Antecedent soil moisture; CN- θ_o relationship; Optimized λ value; SCS-CN

1. INTRODUCTION

The National Engineering Handbook (NEH-4) Soil Conservation Service-Curve Number (SCS-CN) method (SCS 1972) also known as Natural Resource Conservation Service Curve Number (NRCS-CN) method is one of the most popular methods for computing the volume of direct surface runoff for a given rainfall event. It is a two-parameter, initial abstraction (I_a) and CN (or potential maximum retention, S), model to predict surface runoff from rainfall of individual events.

For watershed hydrology, the initial abstraction ratio ($\lambda = I_a/S$) plays an important role in determination of

surface runoff depth (Baltas et al. 2007). It largely depends on climatic conditions of the watershed (Ponce and Hawkins 1996) and consists mainly of interception, infiltration, and surface depression storage during the early parts of a storm (Taguas et al. 2015). Traditionally (SCS 1972) is often set equal to 0.2 in SCS-CN equation. However, use of $\lambda = 0.2$ was called ambiguous by several researchers since its inception (Aron et al. 1977; Baltas et al. 2007; Cazier and Hawkins 1984; D'Asaro and Grillone 2012; D'Asaro et al. 2014; Elhakeem and Papanicolaou 2009; Fu et al. 2001; Hawkins and Khojeini 2000; Hawkins et al. 2002; Shi et al. 2009; Yuan et al. 2014; Zhou and Lei 2011) and a value in the order of 0.05 or less was said to be more realistic not only for the various parts of world, but also for the watersheds those used in its derivation i.e. U.S. watersheds.

For a set of observed P–Q data, various approaches for determining CN have been cited in literature. The most common and widely used are NEH-4 median method; traditionally recommended by SCS (Hawkins et al. 2009; SCS 1972), least-squares method (LSM) (Hawkins et al. 2002), and asymptotic fitting method (AFM) (Hawkins 1993; Hawkins et al. 2009). Of late, some studies examined the relative accuracy of such methods and compared them with those from NEH-4 tables (D'Asaro et al. 2014; Fennessey 2000; Hawkins 1984; Hawkins and Ward 1998; Titmarsh et al. 1989, 1995, 1996; Schneider and McCuen 2005; Tedela et al. 2012). However, in spite of widespread use of all the approaches, there is not an agreed procedure for estimating the CN from observed rainfall–runoff data (Soulis and Valiantzas 2013) because each procedure is as good as another.

Though SCS-CN method has been used worldwide for rainfall runoff modeling, but a common problem encountered is the absence of significant relationship between antecedent soil moisture and measured CN values. The existing SCS-CN method uses the 5-day antecedent rainfall amount to select three AMC levels. However, the use of three discrete AMC levels implies a sudden jump in CN from one level to another (Hawkins 1978). The measured values of CN however are not limited to the three AMC levels defined by 5-day antecedent rainfall (Rallison and Cronshey 1979). Melone et al. (2001) obtained poor results with errors in surface runoff volume up to 100% when used 5-day antecedent rainfall as antecedent wetness condition (AWC) and similar type of results were obtained by other investigators (Beck et al. 2009; Hawkins and Cate 1998; Kottegoda et al. 2000). Therefore, an alternative solution to characterize AWC should be investigated as the use of direct measurements of soil moisture prior to rainfall event, rather than the amount of rainfall only (Brocca et al. 2009; Huang et al. 2007).

Thus, the objective of this study is to (a) investigate the suitability of NEH-4 CN values for agricultural plots; (b) determine the optimal λ and S (or CN) values by analyzing 21 plot data; and finally (c) explore the existence of a relationship between CN (or S) and AWC.

2. SCS-CN METHOD

The SCS-CN method is an empirical equation predicting runoff from rainfall using a parameter CN (or S) based on soil, vegetation, land use, and soil moisture prior to a rainfall event. It is expressed mathematically as:

$$Q = \frac{(P - \lambda S)^2}{(P + S - \lambda S)} \quad \text{for } P > \lambda S; Q = 0 \text{ otherwise} \quad (1)$$

where Q (mm) is surface runoff, P (mm) is rainfall, λ is the initial abstraction ratio ($\lambda = 0.2$ recommended by SCS), and S (mm) is the potential maximum retention. For observed P-Q data, S can be estimated from Eq. 1 as (Hawkins 1973):

$$S = 5[(P + 2Q) - (4Q^2 + 5PQ)^{1/2}] \quad (2)$$

Since parameter S can vary in the range of $0 \leq S < \infty$, it is mapped onto a dimensionless curve number CN, varying in a more appealing range $0 \leq CN \leq 100$, using Eq. 3, and vice versa.

$$CN = \frac{25400}{(S + 254)} \quad (3)$$

3. MATERIALS AND METHODS

3.1 Site description

The study was conducted in an experimental field located at $29^\circ 08' N$ and $77^\circ 09' E$, in Roorkee, district Haridwar, Uttarakhand (India) (Figure 1). The study area is a part of the Solani River catchment, which is a sub watershed of Ganga River-the largest river basin in India. The average elevation of the experimental site is about 266 m above mean sea level (amsl) and; situated within the Solani watershed at about 30-60 km south of the foothills of the Himalayas. The climate at the experimental site is sub-tropical type characterized by hot summers and cold winters with an average temperature vary from 20 to 40 °C. The relative humidity varies between 30% to 99%, and average annual PET of the order of 1340 mm. The annual precipitation varies from 1120 to 1500 mm and most of the rainfall (around 70-80 %) occurs during monsoon season (June-October).



Figure 1 Layout of experimental field located in Roorkee, District Haridwar, [Uttarakhand](#), India.

3.2. Experimental setup and data collection

The selected agricultural field for experimental work was divided into plots of 22 m length and 5 m width with three independent variables: soils, land use, and slope/gradient. The experimental work was conducted for three years (August 2012-March 2015) in which experimental plots included four types of vegetative cover: sugarcane, maize, blackgram, and fallow land with slopes of 1%, 3%, and 5%.

The surface runoff generated during rain storms was collected in separate chambers (1m × 1m × 1m) constructed at the downstream end of each plot and the variation in depth of water stored with respect to time was monitored regularly, but manually. Multi-slot (5 slot) devisors were used to reduce the volume of runoff to be measured in the collection chamber. Precipitation was recorded with the help of Tipping Bucket rain gauge installed within the experimental site. In-situ double ring infiltration tests were conducted for classifying of the hydrologic soil group (HSG). The resulting minimum infiltration capacity and corresponding HSGs for different plots are shown in Table 1. Soil water measurements were taken by a portable unit using a 2-wire connector type time domain reflectometry (TDR) probe of the 'Fieldscout TDR-300'. The soil water was sampled every day (at around 9.00 am IST) throughout the study period from the soil surface down to a depth of 20 cm, and these were replicated at three (upstream, middle, and downstream) locations in each of the plots. Statistical comparisons of soil water contents from these three locations did not show significant difference at $p > 0.05$. For each measurement date, a

single soil water content value was computed by averaging the three values.

3.3 Determination of Curve Number

3.3.1 NEH-4 tables Curve Number

The representative AMC-II CN (or CN2) values were derived for all the plots based on land use, soil type, and vegetation using NEH-4 table (SCS 1972) (Table 1). These CN values of a plot are designated as CNT.

3.3.2 NEH-4 median method

The median CN values derived from Equations 2 and 3 using P-Q data are considered as the representative CNs of the field plots at AMC II (Hawkins et al. 2009; SCS 1972). This CN value of a plot is designated as CNm.

3.3.3 Best Fit method

In this method, the parameter S is determined by iterative least squares fitting (or best fit) procedure for both λ and S of the general SCS-CN equation (Eq. 1), consistent with the work of Hawkins et al. (2002). The objective of the fitting is to find the values of λ and S such that the following is a minimum:

$$\sum_{\text{events}} (Q_{\text{obs}} - Q_{\text{cal}})^2 = \sum \left\{ Q_{\text{obs}} - \left[\frac{(P - \lambda S)^2}{(P + (1 - \lambda)S)} \right] \right\}^2 \quad (4)$$

Here, Q_{obs} = observed direct runoff and Q_{cal} = calculated runoff. Notably, each P-Q dataset yields only one value of S, i.e. only one representative value of S (or CN) for a plot. This CN value of a plot is designated as CNLS. Notably, both natural and ordered data series were used to fit, and only large storm events with $P > 15$ mm were used to avoid the biasing effects of small storms towards high CNs. For statistical analysis, only plots having more than 10 rainfall-runoff events were considered for and CN calculation.

3.3.4 Relationship between CN and AWC

It is of common experience that CN is a function of AWC of the watershed, which may refer to the soil moisture prior to rainfall event. To evaluate the effect of AWC on CN (or S), regressions between CN

derived from P-Q dataset and corresponding observed antecedent soil moisture indices such as 1-day antecedent soil moisture (θ_1), 5-day average antecedent soil moisture (θ_5), 5-day antecedent rainfall (P5) were developed, and their dependency on predicted runoff analyzed. The regression analysis used three forms, viz. linear, logarithmic, and exponential, to fit the experimental data as follows:

$$CN = m + n \theta \quad (5)$$

$$CN = m \exp n \theta \quad (6)$$

$$CN = m + n \ln(\theta) \quad (7)$$

where θ is the antecedent soil moisture index, CN is the curve number, \ln is the natural logarithm operator, m and n are two regression coefficients to be estimated.

Table 1 Characteristics of plots and CN values derived using NEH-4 median method, Least square (LS) method and Handbook Table

Plot No.	Land use	Slope (%)	Infiltration capacity (mm/hr)	HSG	No. of events	NEH-4 Table	NEH-4 method (Natural data, $\lambda=0.20$)	Least square fitting method			
								Natural data		Ordered data	
								CN _T	CN _M	CN _{LSn}	λ
1	Maize	5	4.24	B	12	78	81.93	74.91	0.031	76.17	0.046
2	Maize	3	5.52	B	12	78	81.08	80.49	0.208	80.98	0.219
3	Maize	1	1.90	C	12	85	82.67	81.89	0.100	83.60	0.144
4	Fallow	5	12.00	A	12	76	80.66	62.61	0.020	80.7	0.351
5	Fallow	3	6.00	B	12	85	80.97	59.91	0.000	66.61	0.025
6	Fallow	1	10.00	A	12	76	78.93	60.86	0.063	57.16	0.066
7	Blackgram	5	15.22	A	12	66	81.30	79.07	0.114	87.13	0.421
8	Blackgram	3	13.82	A	12	66	80.09	73.13	0.088	79.09	0.197
9	Blackgram	1	5.66	B	12	77	81.33	69.93	0.033	77.81	0.141
10	Sugarcane	5	7.36	B	18	81	82.14	70.79	0.033	81.87	0.228
11	Sugarcane	3	8.77	A	18	72	80.19	77.00	0.124	89.17	0.659
12	Sugarcane	1	6.51	B	18	81	81.36	70.50	0.000	80.23	0.127
13	Sugarcane	5	2.68	C	10	88	92.35	85.36	0.000	85.97	0.000
14	Sugarcane	3	3.50	C	10	88	90.06	79.03	0.000	79.88	0.000
15	Sugarcane	1	3.03	C	10	88	87.81	74.56	0.000	76.17	0.000
16	Maize	5	10.00	A	15	67	81.52	62.39	0.000	64.06	0.000
17	Maize	3	35.00	A	15	67	80.02	58.13	0.000	58.65	0.000
18	Maize	1	22.00	A	15	67	82.47	70.93	0.000	75.77	0.042
19	Sugarcane	5	32.00	A	15	67	79.83	56.94	0.000	57.21	0.000
20	Sugarcane	3	10.00	A	15	67	86.28	64.47	0.000	67.69	0.004
21	Sugarcane	1	15.00	A	15	67	85.58	61.23	0.000	62.22	0.000
Statistics											
Mean						75.57	82.79	70.20	0.039	74.67	0.127
Median						76.0	81.36	70.79	0.000	77.81	0.046
Standard deviation						8.22	3.57	8.58	0.057	10.11	0.173
Maximum						88.00	92.35	85.36	0.208	89.17	0.659
Minimum						66.00	78.93	56.94	0.000	57.16	0.000

To validate the existence of such a relation, the randomized series of the total collected events were generated to represent fair coverage of all wetness situations. The 60 and 40% events were used for respectively, calibration and validation purpose.

4. PERFORMANCE EVALUATION CRITERIA

For evaluation of the agreement between observed and predicted parameters, three criteria were used

to estimate the goodness of fit, i.e. Nash-Sutcliffe efficiency coefficient (E), coefficient of determination (R²), and bias (e).

The Nash and Sutcliffe efficiency (E) (Nash and Sutcliffe 1970) is defined as:

$$E = \left(1 - \frac{\sum_i^n (Q_i - Q_{ci})^2}{\sum_i^n (Q_i - \bar{Q})^2} \right) \quad (8)$$

where E is the model efficiency, Q_i (mm) and Q_{ci} (mm) are respectively the observed and predicted runoff for storm event i, n is the total number of storm events, and \bar{Q} (mm) is the average of observed runoff for all storm events. E=1 indicates a perfect agreement between observed and predicted values, and its decreasing values indicate poor agreement. A negative value of E can also occur for biased estimates which indicate that the mean observed runoff is a better estimate than calculated runoff.

Bias (e) is a measure of the systematic error and is calculated as the average difference between the predicted and measured values of a random variable as follows:

$$e = \frac{\sum_{i=1}^n (Q_{ci} - Q_i)}{n} \quad (9)$$

The bias indicates the amount that a method consistently over predicts or under predicts the Q-value. Two-way least square fitting was performed to determine the fitting parameters using the Microsoft Excel (Solver).

5. RESULTS AND DISCUSSION

The rainfall-runoff analysis presented in this study is based on the natural rainfall-runoff events observed during August 2012–March 2015. The total number of rainfall events captured was 101 with rainfall amount varying from 1.1 mm to 93.8 mm. However, only 43 events produced significant runoff for measurement. The characteristics and derived CN from various runoff plots are given in Table 1.

5.1 Comparison between CN_T , CN_m and CN_{LS}

In present study, one of the aims was to compare the NEH-4 table curve number (CN_T) with observed P–Q data based curve number. Practically, the NEH-4 table estimates (CN_T) should much close to the P–Q data based CNs. But, in realities, the present comparison is compromised by several factors like equal size and one site location (or same climatic condition) of study plots.

The NEH-4 table curve numbers (CN_T) is compared with those due to P–Q data, observed on 21 plots. The NEH-4 table curve numbers were range from 66 to 88. Observed P–Q data median CNs were range from 78.93 to 92.35. Similarly, the optimized value of CNs ranged respectively from 56.94 to 85.36, and 57.16 to 89.17 for natural and ordered datasets. As seen from Table 1, estimated CN derived for the measured P–Q data set were comparatively higher than that derived for the watershed characteristics.

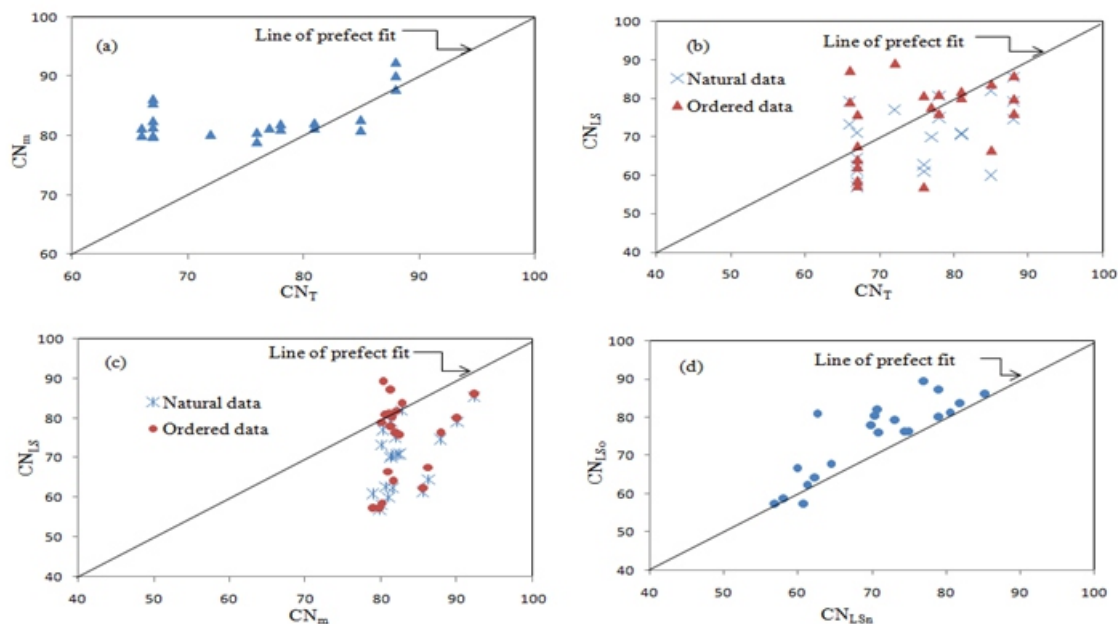


Figure 2 CN Plots for (a) CN_m vs CN_T , (b) CN_{LS} vs CN_T , (c) CN_m vs CN_{LS} , and (d) CN_{LS_o} vs CN_{LS_n} .

From Figure 2a, it is seen that the comparison between CN_{HT} and CN_m is less than satisfactory. Furthermore, CN_m obtained by traditional median method assume high values compared to CN_T and the discrepancy increases for CNs below 75. Most of the CN_m values (17 out of 21) were greater than the CN_T values, consistent with those reported in literature (D'Asaro et al. 2014; Hawkins and Ward 1998).

As shown in Figure 2b, the comparison between CN_T and CN_{LS} is also poor for both natural and ordered datasets. In general, CN_T values are higher than CN_{LS} . Figure 2c shows a plot between CN_m and CN_{LS} for both natural and ordered datasets. The difference is noticeable between CN_m and CN_{LS} for lower CN values. As shown in Tables 1 and Figure 2c, CN_m are higher than CN_{LS} , consistent with those reported

in literature (D'Asaro and Grillone 2012; D'Asaro et al. 2014; Stewart et al. 2012). As expected, CN values derived from ordered data (CN_{LSo}) are higher than CN values derived from natural data (CN_{LSn}) (Figure 2d, Table 1) (D'Asaro and Grillone 2012; D'Asaro et al. 2014; Hawkins et al. 2009; Stewart et al. 2012). It is for obvious reasons that the former CN values derived from frequency matched P and Q data will always be higher than the latter ones derived from natural data as Q corresponding to a P of certain frequency will always be higher than or equal to the observed Q.

Table 2 shows the performance statistic used to test the accuracy of all three sets of CNs, viz., CN_T , CN_m and CN_{LSn} , for the data of 12 plots (plots 1–12 of Table 1), along with resulting R^2 and E values. As seen from this table, CN_T values derived from plot characteristics do not estimate the runoff from these plots as accurately as do the other CNs. For example, CN_{LSn} generally performed the best of all, and CN_m generally better than CN_T . The reason for CN_T to have performed most poorly is that these are the generalized values derived from the watersheds of United States.

From Figures 2a and 2b and Tables 1 and 2, it is evident that the general agreement between CN_T and CN_m or CN_{LSn} is poor, consistent with the results of other studies (D'Asaro et al. 2014; Fennessey 2000; Hawkins 1984; Hawkins and Ward 1998; Lal et al. 2015; Titmarsh et al. 1989, 1995, 1996; Tedela et al. 2012).

Table 2 Performance statistic for runoff estimation using CN_m , CN_{LSn} and CN_T .

Plot No.	Median (Natural data, $\lambda=0.20$)			Least square (Natural data)				NEH-4 Table ($\lambda=0.20$)		
	CN_m	R^2	E	CN_{LSn}	λ	R^2	E	CN_T	R^2	E
1	81.93	0.866	0.624	74.91	0.031	0.910	0.713	78	0.805	0.321
2	81.08	0.948	0.700	80.49	0.208	0.941	0.638	78	0.921	0.474
3	82.67	0.861	0.587	81.89	0.100	0.893	0.740	85	0.884	0.731
4	80.66	0.686	0.625	62.61	0.020	0.712	0.649	76	0.597	0.357
5	80.97	0.545	0.474	59.91	0.000	0.611	0.584	85	0.601	0.551
6	78.93	0.690	0.650	60.86	0.063	0.682	0.640	76	0.641	0.496
7	81.30	0.750	0.525	79.07	0.114	0.773	0.588	66	0.025	-0.264
8	80.09	0.790	0.592	73.13	0.088	0.806	0.599	66	0.013	-0.231
9	81.33	0.736	0.592	69.93	0.033	0.766	0.611	77	0.660	0.305
10	82.14	0.571	0.514	70.79	0.033	0.595	0.494	81	0.543	0.451
11	80.19	0.490	0.387	77.00	0.124	0.501	0.404	72	0.154	-0.042
12	81.36	0.516	0.390	70.50	0.000	0.563	0.507	81	0.505	0.365

5.2 Derivation of Initial abstraction ratio (λ) values

The optimized λ –values derived for both natural and ordered P–Q data sets are shown in Table 1. As seen from this table, the derived initial abstraction ratio (λ) values vary widely (ranging from 0 to 0.659 for ordered data and 0 to 0.208 for natural data) from plot to plot with 0 as the most frequent value. The most of the derived λ values (respectively 20 and 16 out of 21 for natural and ordered P–Q data sets)

are less than the default $\lambda=0.2$ value. The mean and median λ values were respectively 0.039 and 0 for natural P-Q data, and 0.127 and 0.046 for ordered P-Q data, which is quite different from traditionally assumed value, but consistent with those reported in literature (Baltas et al. 2007; D'Asaro and Grillone 2012; D'Asaro et al. 2014; Elhakeem and Papanicolaou 2009; Fu et al. 2011; Hawkins and Khojeini 2000; Hawkins et al. 2002; Shi et al. 2009; Yuan et al. 2014; Zhou and Lei 2011).

I_a was plotted against S , using the whole data of 21 plots as shown in Figure 3. The I_a - S plot exhibited an inverse relationship for both natural and ordered data sets, consistent with the findings by Jiang (2001). The regression equations were $I_a = -3.21 \ln(S) + 18.13$, $R^2=0.10$ for natural data, and $I_a = -7.30 \ln(S) + 38.94$, $R^2=0.30$ for ordered data. The R^2 was significant at $p<0.05$ for both ordered and natural data sets. This result from current study conflicts with the suggested linear positive relationship between I_a and S ($I_a=0.2S$) as suggested by the NRCS Curve Number model, but consistent with findings carried out elsewhere (Elhakeem and Papanicolaou 2009; Jiang 2001; Jain et al. 2006; Mishra et al. 2004, 2006).

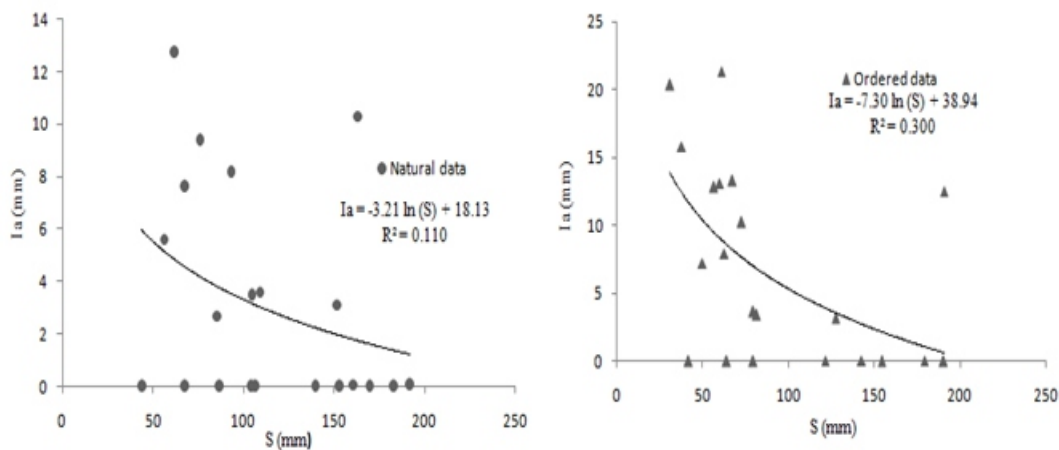


Figure 3 Relationship between I_a and S for 21 plot-data.

5.3 Effect of AWC on CN (or S)

Table 3 compares the performance of four soil moisture indices with three different regression models for improved runoff estimation. As seen, the exponential regression of CN with θ_{o1} (i.e. $CN=69.905 \exp^{0.00776\theta_{o1}}$) performed the best of all in both calibration and validation. However, the existing index based on 5-day antecedent rainfall (P_5) exhibited a poor performance in comparison to one day antecedent moisture (θ_{o1}), consistent with the results reported elsewhere (Brocca et al. 2008, 2009; Beck et al. 2009).

Table 3 Performance of various relations between CN and AWC indices

	1-day antecedent soil moisture (θ_{01})			5-day average antecedent soil moisture (θ_{05})			5-day antecedent rainfall (P_5)		
	R ²	E	e (mm)	R ²	E	e (mm)	R ²	E	e (mm)
Linear regression model (Eq. 5)									
Calibration	0.737	0.610	0.51	0.704	0.460	0.85	0.708	0.511	0.56
Validation	0.835	0.726	0.96	0.829	0.649	1.37	0.816	0.699	1.06
Exponential regression model (Eq. 6)									
	CN=69.905exp ^{0.00776θ_{01}}			CN=74.617exp ^{0.00586θ_{05}}			CN=79.82exp ^{0.0011P₅}		
Calibration	0.736	0.620	0.39	0.709	0.476	0.71	0.709	0.532	0.36
Validation	0.837	0.737	0.83	0.829	0.674	1.13	0.817	0.716	0.84
Logarithmic regression model (Eq. 7)									
Calibration	0.730	0.560	0.74	0.703	0.451	0.90	0.708	0.441	0.83
Validation	0.830	0.686	1.26	0.829	0.640	1.38	0.816	0.632	1.54

Table 4 shows the performance statistic used to test the accuracy of developed relationships of CN with θ_{01} (i.e. $CN=69.905exp^{0.00776\theta_{01}}$) and P_5 (i.e. $CN=79.82exp^{0.0011P_5}$) in estimation of runoff, for the data of 6 plots (plots 7–12 of Table 1), along with resulting R² and E values. As seen, $CN=69.905exp^{0.00776\theta_{01}}$ was found to produce better runoff estimates as compared to $CN=79.82exp^{0.0011P_5}$ for 5 out of 6 plot datasets.

Table 4 Performance statistic for runoff estimation using CN relationship with θ_{01} and P_5

Plot	CN=69.905exp ^{0.00776θ_{01}}		CN=79.82exp ^{0.0011P₅}	
	R ²	E	R ²	E
7	0.920	0.898	0.897	0.827
8	0.863	0.744	0.862	0.711
9	0.800	0.544	0.780	0.606
10	0.812	0.796	0.710	0.699
11	0.722	0.678	0.675	0.673
12	0.807	0.702	0.694	0.677

6. CONCLUSIONS

The following conclusions can be derived from the present experimental study involving various land uses (fallow, maize, blackgram and sugarcane) on soils of different hydrologic soil groups (HSG) and plot slopes ranging from 1% to 5%.

- The CNs derived for NEH–4 tables based on plot characteristics do not match well with CNs derived for observed P–Q data.
- The optimized λ values showed that the original assumption of the initial abstraction ratio (λ) of 0.20 is unusually high. The mean and median λ values were respectively 0.039 and 0 for natural P–Q data, and 0.127 and 0.046 for ordered P–Q data. Ia-S relation was non-linear.

- CN showed greater dependence on the physically measured 1-day antecedent soil moisture (θ_{01}) than the other soil moisture indices considered in this study.

ACKNOWLEDGMENTS

This research was funded by the Indian National Committee on Surface Water (INCSW) (formerly Indian National Committee on Hydrology (INCOH)), and Ministry of Water Resources, Govt. of India, New Delhi under the Research and Development project (MOW-627-WRD) on “Experimental Verification of SCS Runoff Curve Numbers for Selected Soils and Land Uses”.

REFERENCES

- Aron, G., Miller AC, and Lakatos, D. F. (1977). Infiltration formula based on SCS curve number. *Journal of Irrigation and Drainage Division*, 103(4):419–427.
- Baltas, E. A., Dervos, N. A., and Mimikou, M. A. (2007). Determination of the SCS initial abstraction ratio in an experimental watershed in Greece. *Hydrological Earth System Science*, 11:1825-1829.
- Beck, H. E., Jeu, R. A. M., Schellekens, J., Van Dijk, A. I. J. M., and Bruijnzeel, L. A. (2009). Improving curve number based storm runoff estimation using soil moisture indices. *J. Sel. Topics Appl. Earth observations in Remote Sensing*, 2(4), 250-259.
- Brocca, L., Melone, F., and Moramarco, T. (2008). On the estimation of antecedent wetness conditions in rainfall runoff modeling. *Hydrological Processes*, 22, 629-642.
- Brocca, L., Melone, F., Moramarco, T., and Singh, V. P. (2009). Assimilation of observed soil moisture data in storm rainfall-runoff modeling. *Journal of Hydrologic Engineering*, 14, 156-164.
- Cazier, D. J., and Hawkins, R. H. (1984). Regional application of the curve number method. *Proc., Water Today and Tomorrow, ASCE Irrigation and Drainage Division Special Conf., ASCE, Reston, VA.*
- D'Asaro, F., and Grillone, G. (2012). Empirical investigation of curve number method parameters in the Mediterranean area. *Journal of Hydrologic Engineering*, 17:1141-1152.
- D'Asaro, F., Grillone, G., and Hawkins, R. H. (2014.) Curve Number: Empirical Evaluation and Comparison with Curve Number Handbook tables in Sicily. *Journal of Hydrologic Engineering*, 19(12):04014035 (1-13).
- Elhakeem, M., and Papanicolaou, A. N. (2009). Estimation of the runoff curve number via direct rainfall simulator measurements in the state of Iowa, USA. *Water Resource Management*, 23(12):2455-2473.
- Fennessey, L. A. (2000). The effect of inflection angle, soil proximity and location on runoff. Ph.D. dissertation, Pennsylvania State University, State College, PA.
- Fu, S., Zhang, G., Wang, N., and Luo, L. (2011). Initial abstraction ratio in the SCS-CN method in the Loess Plateau of China. *Trans ASABE*, 54(1):163–169.
- Hawkins, R. H. (1973). Improved prediction of storm runoff in mountain watershed. *Journal of Irrigation and Drainage Division*, 99:519-523.
- Hawkins, R. H. (1984). A comparison of predicted and observed runoff curve numbers. *Symposium, Proceeding, Water Today and Tomorrow, ASCE, Reston, VA*, 702-709.
- Hawkins, R. H. (1993). Asymptotic determination of runoff curve numbers from data. *Journal of Irrigation and Drainage Engineering*, 119(2):334-345.
- Hawkins, R. H., Jiang, R., Woodward, D.E., Hjelmfelt, A.T., van Mulle., J. A., and Quan, Q. D. (2002). Runoff curve number method: Examination of the initial abstraction ratio, in *Proceedings of the Second Federal Interagency Hydrologic Modeling Conference, ASCE Publications: Las Vegas.*
- Hawkins, R. H., and Khojeini, A.V. (2000). *Initial Abstraction and Loss in the Curve Number Method. Arizona. Hydrological Society Proceedings.*
- Hawkins, R. H., and Ward, T. J. (1998). Site and cover effects on event runoff, *Jornada experimental range, New Mexico. Symp. Proc., Conf. on Rangeland Management and Water Resources, American Water Resources Associations, Middleburg, VA*, 361-370.
- Hawkins, R. H., Ward, T. J., Woodward, D. E., and Van Mullem, J. A. (2009). *Curve number hydrology: State of practice, ASCE, Reston, VA*, 106.
- Hawkins, R. H. (1978). Runoff curve numbers with varying site moisture. *Journal of Irrigation and Drainage Division*, 104, 389–398.

- Hawkins, R.H., and Cate, A.J. (1998). Secondary effects in curve number rainfall-runoff. Presented at Water Resources Engineering 98, Memphis Tennessee, August 3-7.
- Huang, M., Gallichand, J., Dong, C., Wang, Z., and Shao, M. (2007). Use of soil moisture data and curve number method for estimating runoff in the Loess Plateau of China. *Hydrological Processes*, 21(11), 1471-1481.
- Jain, M. K., Mishra, S. K., Babu, P., Suresh, Venugopal, K., and Singh, V. P. (2006). An enhanced runoff curve number model incorporating storm duration and non-linear Ia-S relation. *Journal Hydrologic Engineering*, 11(6):631-635.
- Jiang, R. (2001). Investigation of Runoff Curve Number Initial Abstraction Ratio. MS Thesis Watershed Management, University of Arizona. pp.120.
- Kottegoda, N.T., Natale, L., and Raitieri, E. (2000). Statistical modeling of daily stream flows using rainfall input and curve number technique. *Journal of Hydrology*, 234, 170-186.
- Lal, M., Mishra, S. K., and Pandey, A. (2015). Physical verification of the effect of land features and antecedent moisture on runoff curve number. *Catena*, 133:318-327.
- Melone, F., Neri, N., Morbidelli, R., and Saltalippi, C. (2001). A conceptual model for flood prediction in basins of moderate size. *Applied simulation and modeling*, M. H. Hamza, ed., IASTED Acta Press, Anaheim, Calif., 461-466.
- Mishra, S. K., Jain, M. K., and Singh, V. P. (2004). Evaluation of SCS-CN-based model incorporating antecedent moisture. *Water Resource Management*, 18(6):567-589.
- Mishra, S. K., Sahu, R. K., Eldho, T. I., and Jain, M. K. (2006). An improved Ia-S relation incorporating antecedent moisture in SCS-CN Methodology. *Water Resource Management*, 20(5):643-660.
- Nash, J. E., and Sutcliffe, J.E. (1970). Modeling infiltration during steady rain. *Water Resource Research*, 9, 384-394.
- Ponce, V. M., and Hawkins, R. H. (1996). Runoff curve number: has it reached maturity? *Journal of Hydrologic Engineering*, 1(1):11-19.
- Rallison, R. E., and Cronshey, R. C. (1979). Discussion to 'Runoff curve numbers with varying soil moisture'. *Journal of Irrigation and Drainage Division*, 105, 439-441.
- Schneider, L. E., and McCuen, R. H. (2005) Statistical Guidelines for Curve Number Generation. *Journal of Irrigation and Drainage Engineering*, 131(3):282-290.
- SCS. (1972). 'Hydrology' National Engineering Handbook, Supplement A, Section 4, Soil Conservation Service, USDA, Washington, DC.
- Shi, Z. H., Chen, L. D., Fang, N. F., Qin, D. F., and Cai, C. F. (2009), Research on the SCS-CN initial abstraction ratio using rainfall-runoff event analysis in the Three Gorges Area, China. *Catena* 77:1-7.
- Soulis, K. X., and Valiantzas, J. D. (2013), Identification of the SCS-CN parameter spatial distribution using rainfall-runoff data in heterogeneous watersheds. *Water Resource Management*, 27(6):1737-1749.
- Stewart, D., Canfield, E., and Hawkins, R. H. (2012). Curve number determination methods and uncertainty in hydrologic soil groups from semiarid watershed data. *Journal of Hydrologic Engineering*, 17:1180-1187.
- Taguas, E., Yuan, Y., Licciardello, F., and Gómez, J. (2015). Curve Numbers for Olive Orchard Catchments: Case Study in Southern Spain. *Journal of Irrigation and Drainage Engineering*, DOI: [10.1061/\(ASCE\)IR.1943-4774.0000892](https://doi.org/10.1061/(ASCE)IR.1943-4774.0000892).
- Tedela, N. H., McCutcheon, S. C., Rasmussen, T. C., Hawkins, R. H., Swank, W. T, Campbell, J. L., Adams, M. B., Jackson, C. R., and Tollner, E. W. (2012). Runoff Curve Numbers for 10 Small Forested Watersheds in the Mountains of the Eastern United States. *Journal of Hydrologic Engineering*, 17(11):1188-1198.
- Titmarsh, G. W., Cordery, I., and Pilgrim, D. H. (1995). Calibration procedures for rational and USSCS design hydrographs. *Journal of Hydraulic Engineering*, 121(1):61-70.
- Titmarsh, G. W., Cordery, I., and Pilgrim, D. H. (1996). Closure of calibration procedures for rational and USSCS design flood methods. *Journal of Hydraulic Engineering*, 122(3):177.
- Titmarsh, G. W., Pilgrim, D.H., Cordery, I., and Hossein, A. A. (1989). An examination of design flood estimations using the U.S. soil conservation services method. *Hydrology and Water Resources Symposium*, Institution of Engineers, Barton, ACT, Australia.
- Yuan, Y., Nie, J., McCutcheon, S. C., and Taguas, E. V. (2014). Initial abstraction and curve numbers for semiarid watersheds in south eastern Arizona. *Hydrological Processes*, (28):774-783.
- Zhou, S. M., and Lei, T. W. (2011). Calibration of SCS-CN Initial Abstraction Ratio of a typical small watershed in the Loess Hilly-Gully region. *China Agriculture Science*, (44):4240-4247.

Static And Dynamic Behaviors Of Geocell Reinforced Soft Clay

¹Ashim Kanti Dey, ²Prasenjit Debnath,

¹Professor, Department of Civil Engineering, NIT Silchar, Silchar- 788010,

E-mail ashim_kanti@yahoo.co.in

²M.Tech research scholar, Department of Civil Engineering, NIT Silchar, Silchar- 788010,

E-mail prasen458@gmail.com

ABSTRACT

Soft clay is normally avoided during construction due to its low bearing capacity and high susceptibility of consolidation. The safe bearing capacity of soft clay is considerably increased with insertion of geocells at a suitable depth from the foundation level. Although it is known that geocell reinforced soft clay behaves differently in confined and unconfined conditions, but a detailed study is not reported yet. Moreover, the behavior of geocell reinforced soft clay under dynamic loading is also not properly studied. Extent of increase in bearing capacity of soft clay due to insertion of geocells is also not known. Present research is intended to carry out a series of static and cyclic triaxial tests in confined and unconfined conditions and to understand the effect of geocells on modification of strength parameters and dynamic properties of soft clay. It is observed that under unconfined conditions, the geocells will compress resulting in increase in strain, whereas, under confined condition, the geocells will stiffen the soil resulting in increase in stress. It is also observed that maximum improvement in axial stress is achieved when the geocells are placed at a depth of one fourth of the loading diameter. However, position of geocells does not have a significant effect on stress strain curve in unconfined condition. The stress strain curve of geocell reinforced clay shows an early rise in stress. It is observed that the shear modulus increases and the damping ratio decreases due to insertion of geocells in soft clay.

1. INTRODUCTION

During the last three decades geosynthetics are being extensively used to improve the properties of poor soil, like to increase the drainage property, to reduce the compressibility, to improve the shear strength, etc. In order to increase the bearing capacity of soft clay, use of geocells is also being extensively used [Bush et al., 1990], [Cowland and Wong, 1993], [Hendricker et al., 1998], [Dash, et.al., 2001], [Leshchinsky and Ling, 2013], [Fakher and Jones, 1996], [Madhavi and Vidya, 2007], [Selig and McKee, 1961], and so on. Dash et al. (2003) reported that provision of geocell reinforcement improves the load carrying capacity of foundation soil. Normally a geocell is a three-dimensional, honey-comb like structure made of geosynthetics interconnected by joints. Geogrids are normally used to make the

the cage and geotextiles or geomembranes are put inside the cage for retaining the filling material like sand, gravel or boulder. The geocells may be triangular, square, rectangular or hexagonal in plan depending upon the nature of utility. Geocells have been found to be useful for base reinforcement of embankments and subgrade soil, reinforcement below shallow foundations and steep slopes and in other applications where the soil should withstand high tensile stresses. Flexural rigidity of the geocells plays an important role in increasing the strength of soil against bending. In the present study, effects of geocells in modifying the shear strength of soft clay under static and dynamic loading have been undertaken. A series of triaxial compression tests have been carried out on 75 mm diameter clayey soil samples reinforced with four interconnected geocells placed at different depths from the top of the sample. Cyclic triaxial tests have also been conducted on the samples to find out the improvement on dynamic properties of soft clay, due to insertion of geocells. A considerable improvement in the static and dynamic properties has been observed.

2. MATERIALS USED FOR TESTING

Locally available silty clayey soil which has 60% fines finer than 75 micron was used for the present study. Fig. 1 shows the particle size distribution of this soil. The liquid limit, plastic limit and specific gravity of the soil were found to be 52%, 27% and 2.54 respectively. As per Unified Soil Classification System (USCS), the soil is classified as inorganic clay with high compressibility (CH). The undrained in-situ shear strength of the soil obtained through vane shear test was found to be 6.5 kPa at a density of 20.73 kN/m³ and water content 40.2%. All the laboratory tests were performed on remolded samples prepared through four steps. The steps were to dry the clay lumps, grind the lumps into fine powder, add requisite quantity of water and finally consolidate the sample into the desired density. Water content was tried to keep around 40%. The size of each soil sample was kept as 75 mm diameter x 150 mm height. Four interconnected geocells, each of size 20 x 20 x 20 mm were prepared with geo-grid. A layer of geomembrane (locally available plastic sheet, 0.09 mm thick) was put inside the geogrid. Coarse sand was poured into each cell. Fig. 2 shows the picture of the geocells used in the present study. The geocells were placed at different depths inside the soil sample as shown in Figs. 3 and 4. Table 1 shows the properties of the geogrid. Gradation curve of the coarse sand which was used to fill the geocells is also shown in Fig. 1. The sand has a uniformity coefficient (C_u) of 2.28, coefficient of curvature (C_c) of 1.11 and specific gravity of 2.6. The soil is classified as poorly graded sand with nomenclature SP according to the USCS soil classification system. For all the tests the sand was compacted to a density of around 16 kN/m³ (i.e. 70% relative density) for filling the geocells. Direct shear tests of this density show that the angle of shearing resistance is 39°.

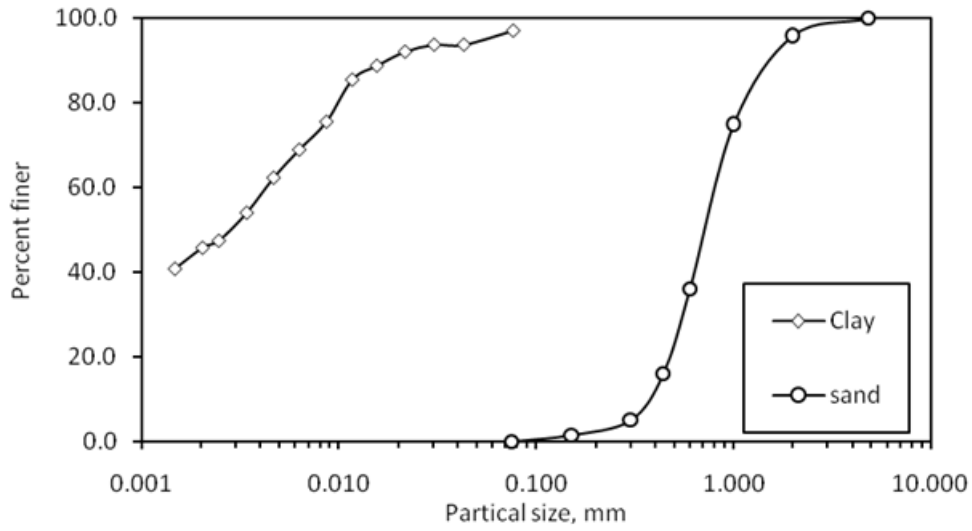


Figure 1 Particle size distribution of the clay and sand used in the study

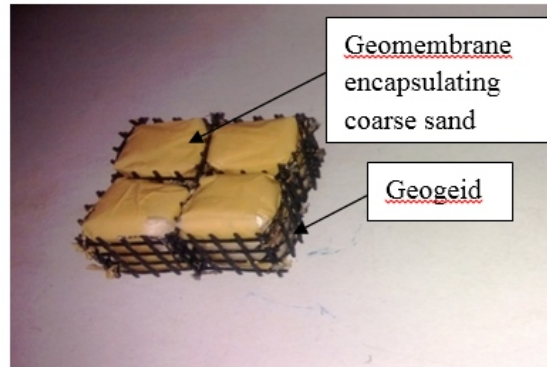


Figure 2 Four interconnected geocells used in the present study

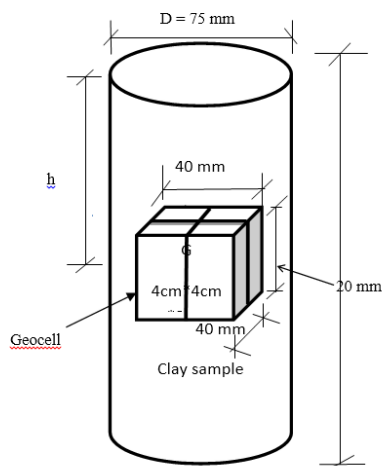


Figure 3 Placement of geocell inside the soil sample

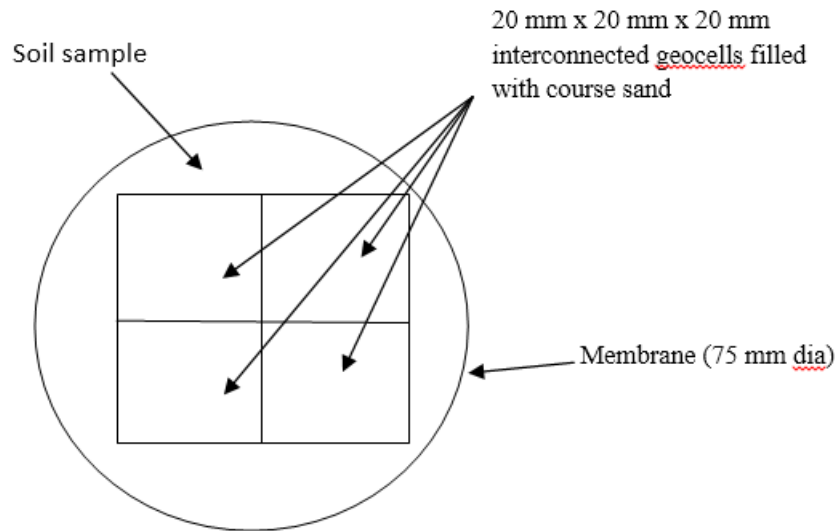


Figure 4 Cross section through soil sample with geocells

Table 1 Properties of the geogrid

Parameter	Value
Polymer	Polypropylene
Aperture size (MD*XMD)	6mm*5mm
Peak tensile strength (MD*XMD)	4.8 <u>kN/m</u> *5.5kN/m
Yield point strain (MD*XMD)	23%*20%
Aperture opening shape	Rectangle

MD: machine direction, XMD: cross-machine direction.

Fig. 5 shows the stress - strain curve of the four geocells containing geomembrane encapsulated sand as shown in figure 2. It is observed that the geocells filled with sand get compressed under a compressive load, follow an elastic path upto around 30% strain, pass through plastic state upto 62% strain and then fail by rupturing. The result suggests the possible use of present form of geocells as an elastic material upto 20% strain.

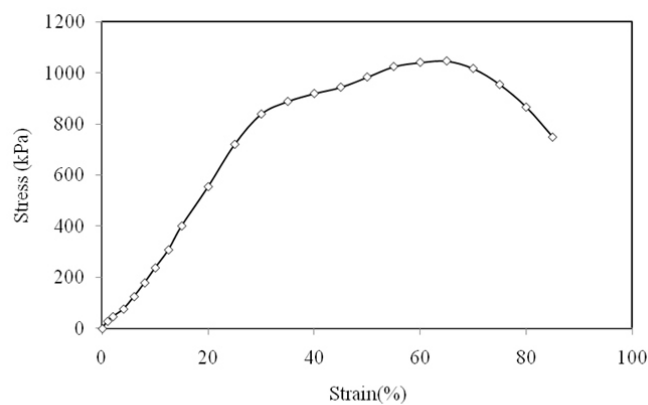


Figure 5 Stress- strain behavior of geocell

3. TEST PROGRAMME

It was decided to conduct both static and cyclic triaxial tests on 75 mm diameter soil samples. In one set of tests a confining pressure of 100 kPa was applied, whereas in other set of tests no confining pressure was applied for obtaining the unconfined compressive strength. In order to obtain the degradation of strength due to cyclic loading, 30 cycles were given to each sample under displacement control mode, with displacement amplitude ± 1 mm and frequency of loading 1 Hz. Soon after the cyclic loading, the sample was sheared under unconsolidated undrained condition to find the degraded shear strength. The position of geocell was varied for different tests. The total test programme is shown in Fig. 6.

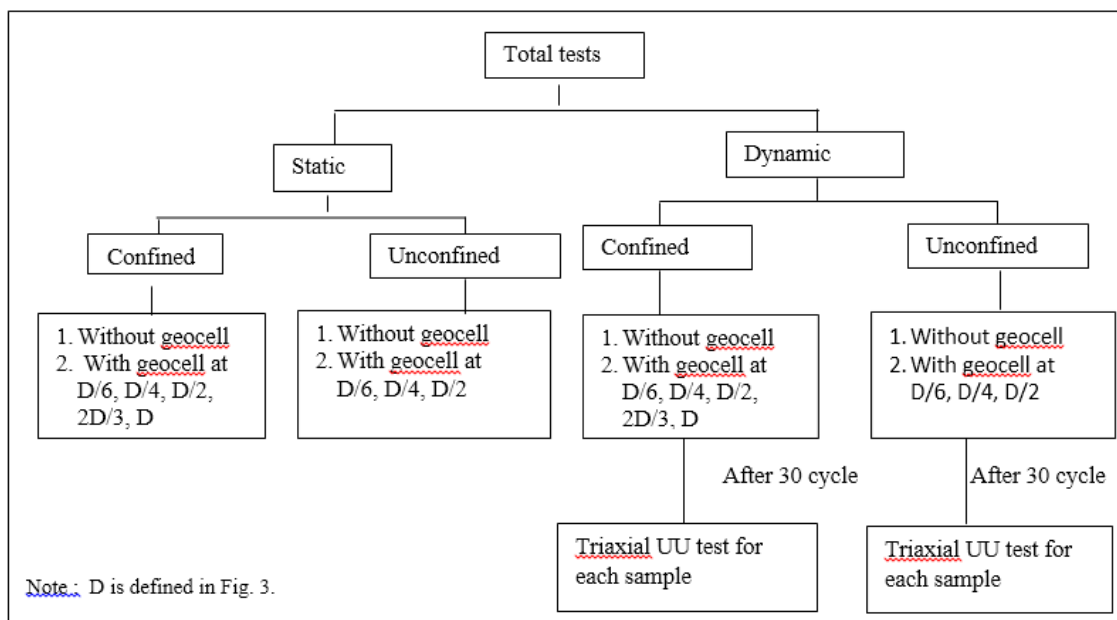


Fig. 6 Test programme.

4. RESULTS AND DISCUSSION

4.1. STATIC TRIAXIAL TEST

Typical stress-strain curves from the static triaxial UU tests with and without confining pressures are shown in Figs. 7 (a) and (b) respectively. The position of geocell from the top of the sample is also shown in the figure. For a comparison purpose, the stress strain curve for the normal soil sample without any geocell is superimposed on the figure. It can be seen that for geocell reinforced soil no failure stress is achieved. However, in this study, a stress corresponding to 20% strain is considered to be the failure stress. In addition to the increase in the strength of soil, there was a corresponding increase in the stiffness of the soil, which is indicated by steeper stress strain curves as in Figs. 7(a) and (b). Rajagopal

. al. 1999 also reported an increase in stiffness of geocell reinforced sand samples. Their results also showed that failure does not occur even at 20% strain. As obvious, the maximum failure stress for geocell reinforced clay is more than that for unreinforced clay. This increase in strength is due to enhanced confinement effect [Bathurst and Karpurapu, 1993]. In the present study maximum increase in deviator stress is observed when the geocell is placed at a depth of $D/4$ from the top of the sample. This may be compared with the results obtained by Dash et. al 2001 who obtained the optimum depth of geocell as $0.1B$ for sandy soil.

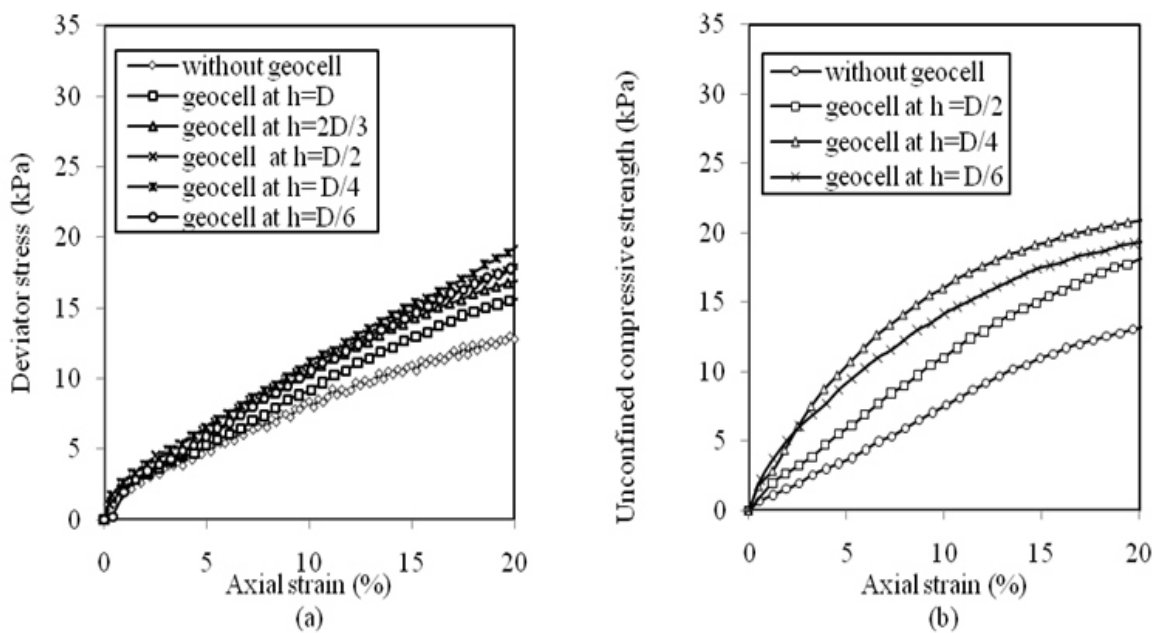


Figure 7 (a) Deviator stress-strain for soil samples with and without geocell with confining pressure = 100 kPa.
 (b) Unconfined compressive strength against strain for soil samples with and without geocell

A term, known as Improvement Factor is defined as a ratio of deviator stress of geocell reinforced soil to that of unreinforced soil corresponding to 20% strain. The variation of improvement factor for the confined and unconfined tests is shown in Figs. 8 (a) and (b) respectively. It is observed that the improvement factor increases with strain for confined tests implying that a properly confined geocell will take a higher load. An unconfined soil on the other hand takes a high load at low strain upto 2 to 3%. At large strain the improvement factor for unconfined soil is around 1.5 irrespective of position of geocells. This indicates that a geocell reinforced clayey soil takes a higher load either in confined or unconfined condition.

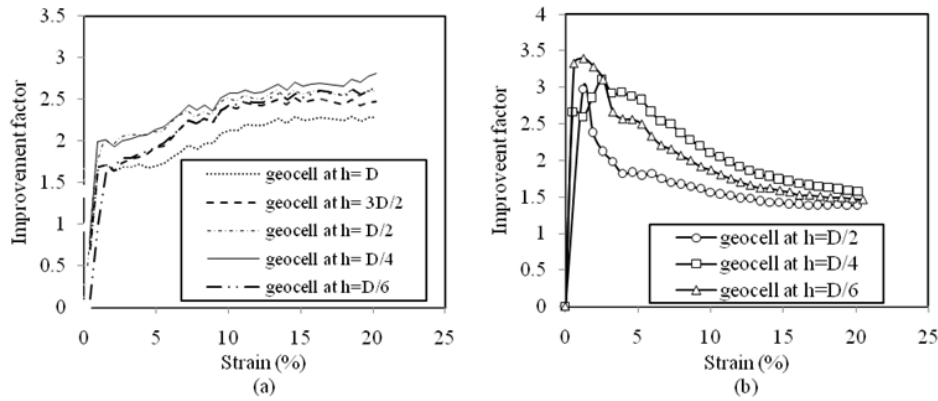


Figure 8 Improvement factor against strain: (a) with confining pressure 100 kPa. (b) Without confining pressure

4.2 CYCLIC TRIAXIAL TEST

Cyclic triaxial tests were conducted on geocell reinforced soil samples with and without confining pressures. 30 load cycles at 1 Hz frequency were applied under displacement control mode with amplitude ± 1 mm. Typical stress strain loops of clayey soil are shown in Figs. 9 and 10 with and without geocells respectively. Seed and Idriss, 1971 gave a concept of equivalent number of uniform load cycles to represent an earthquake; using their concept, 30 number of uniform load cycles indicate an earthquake magnitude of 8. Static triaxial UU tests were conducted on each sample after application of 30 cycles to observe the variation of residual strength due to installation of geocell reinforced soft clay. Variation of deviator stress against strain under static tests is shown in Fig. 11 (a) with confining pressure and variation of unconfined compressive strength against strain in Fig. 11 (b). It is also observed that after cyclic loading, the failure deviator stress is more for geocell reinforced soil than that for unreinforced clay. Maximum increase in deviator stress is observed when the geocell is placed at a depth of $D/4$ from the top of the sample.

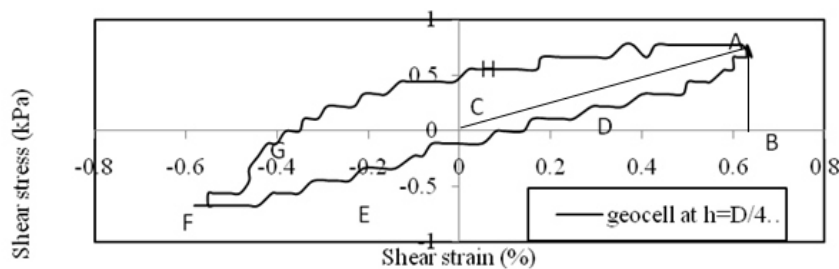


Figure 9 Shear stress - shear strain loop of geocell reinforced clay with confining pressure = 100 kPa.

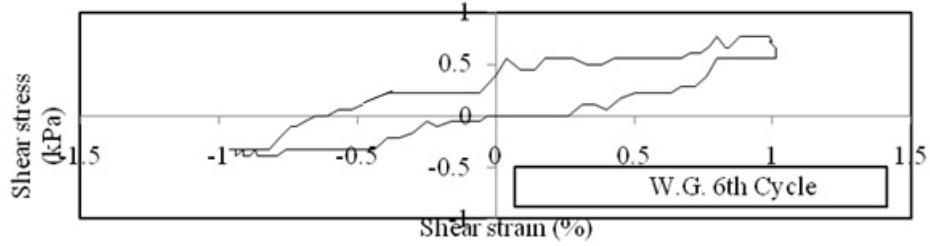


Figure 10 Shear stress - shear strain loop of unreinforced clay with confining pressure = 100 kPa.

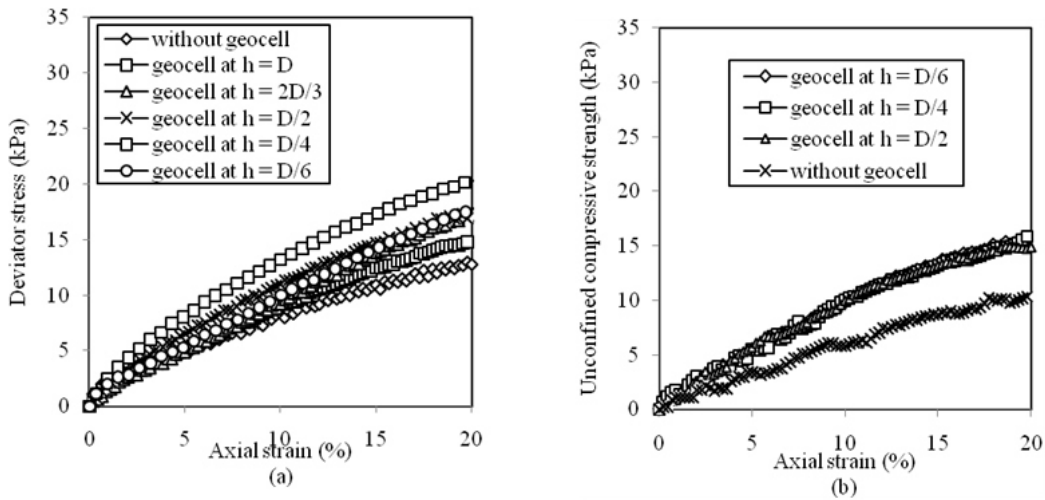


Figure 11 (a) Deviator stress against strain after 30 cycles of loading with confining pressure 100 kPa
(b) Unconfined compressive strength against Strain after 30 cycles of loading.

A comparison of failure deviatoric stress before and after dynamic loading is also made to find the degree of degradation, which is defined as reduction in deviator stress due to cyclic loading to the deviator stress without cyclic loading. It is observed that cyclic loading has degraded the strength of geocell reinforced soil. Table 2 shows the % degradation of axial stress for confined and unconfined tests. It is observed that degradation of normal soft clay is around 4% whereas for geocell reinforced soft clay the degradation is around 2-3% under confined condition except for the case where geocell was placed just below the loading plunger ($h=D/6$), degradation for this position is around 5%. For unconfined condition, geocell reinforced soft clay has a high degradation value, around 15 -20%. Thus the geocells are not effective in reduction of degradation of soft clayey soil under cyclic loading. In unconfined condition the degradation due to installation of geocells are even more than the normal soil. This indicates a limitation of applications of geocells under unconfined condition and placing just below the foundation.

Table 2 Percentage degradation of deviator stress and unconfined compressive strength due to cyclic loading corresponding to 20% strain.

Position of geocell, h (cm)	Confined			Unconfined		
	Deviator Stress (kPa) at 20% strain	Deviator Stress (kPa) at 20% strain after 30 loading cycles	% of degradation	Unconfined compressive strength (kPa) at 20% strain	Unconfined compressive strength (kPa) at 20% strain after 30 loading cycles	% of degradation
h=D/6=1.25	18.64	17.66	5.26	19.13	15.7	17.93
h=D/4=1.875	20.5	20.1	1.95	21.58	16.19	24.98
h=D/2=3.75	17.66	17.17	2.77	17.67	14.72	16.70
h=2D/3=5.00	16.87	16.68	1.13			
h=D=7.50	15.67	15.2	3.00			
Without geocell	12.75	12.26	3.84	12.75	10.79	15.37

Variations of failure deviatoric stress against location of geocell for all the above triaxial tests are shown in Fig 12. From the figure it is observed that the failure deviatoric stress increases with increase in placement depth of geocell from the top; attains a maximum value with geocells at D/4 and then decreases with increase in placement depth. It is thus concluded that the maximum deviatoric stress is obtained when the geocells are placed at D/4 even after a certain number of loading cycles.

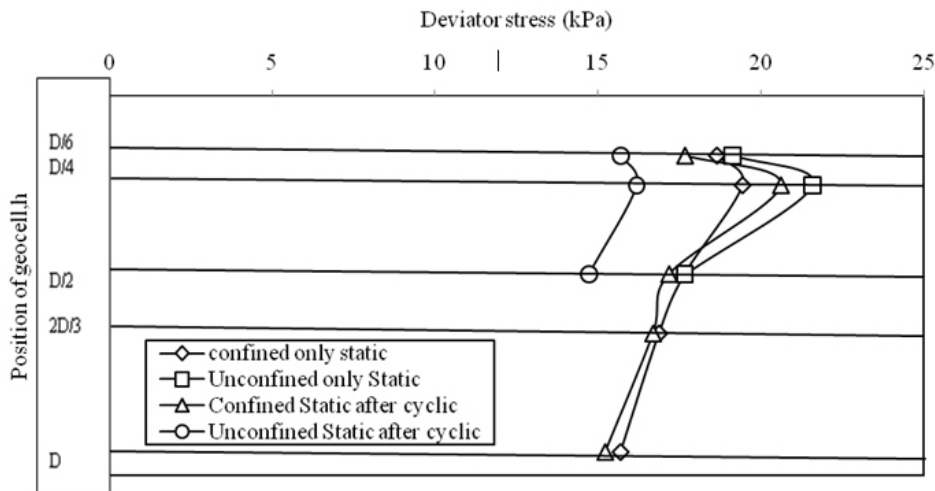


Figure 12 Variation of deviator Stress with position of geocell.

4.3 DYNAMIC TEST RESULTS AND DISCUSSIONS

When a soil is subjected to a cyclic loading, the stress strain curve forms a loop called a hysteresis loop, the area of the loop shows the energy dissipated during a cycle. The loop can be described by two parameters, namely, inclination to the strain axis and width of the loop. The inclination of the hysteresis loop depends upon the stiffness of the soil, and is defined by a term called secant shear modulus, G_{sec} , which is tangent of the angle intercepted by a line joining two vertices of the loop with the strain axis.

Figs. 13 (a) and (b) show the changes of secant shear modulus with the variation of no. of cycles for confined and unconfined cyclic triaxial compression tests. From the graphs it may be clearly seen that when the geocell is at D/4 from the top, the value of secant shear modulus is the highest of all the values. Variation of secant shear modulus against number of cycles for unreinforced soil is also shown in the figures. It can be seen that the secant shear modulus of unreinforced soil is always the lowest for both confined and unconfined conditions.

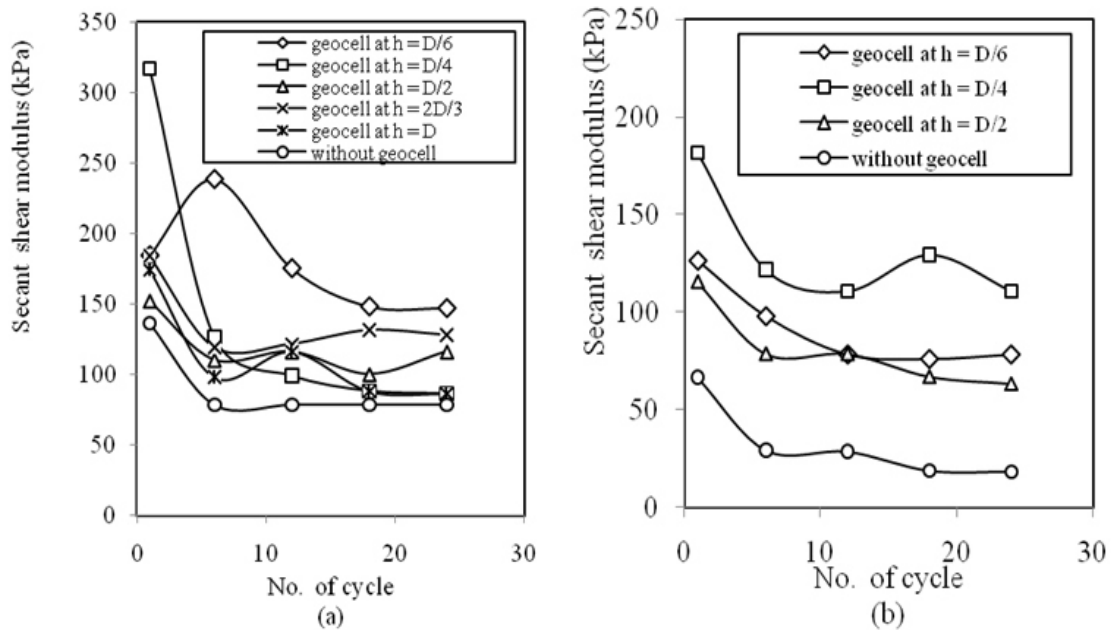


Fig. 13 Secant shear modulus against number of cycles: (a) with confining pressure 100 kPa (b) without confining pressure.

Considering the changes in the value of shear modulus due to placement of geocells, a term named as 'Modification factor' is defined as the ratio of a geocell reinforced soil property to the corresponding unreinforced soil property. Variation of modification factor of secant shear modulus with number of loading cycles for different positions of geocell is shown in Figs. 14 (a) and (b) with and without confining pressures. It is observed that under confined condition, the modification factor does not follow a definite trend for different positions of geocells, whereas under unconfined condition the modification factor shows an increasing trend with number of cycles. This indicates that stiffness of geocell reinforced soft clay increases with increase in number of loading cycles – the maximum increase occurs when the geocell is placed at D/4. The main reason for this increase is due to the fact that under cyclic loading the soft soil compresses under unconfined condition. Although some trend is observed for the modification factor when the geocells are placed at D/4, however, no definite conclusion can be drawn with these few tests.

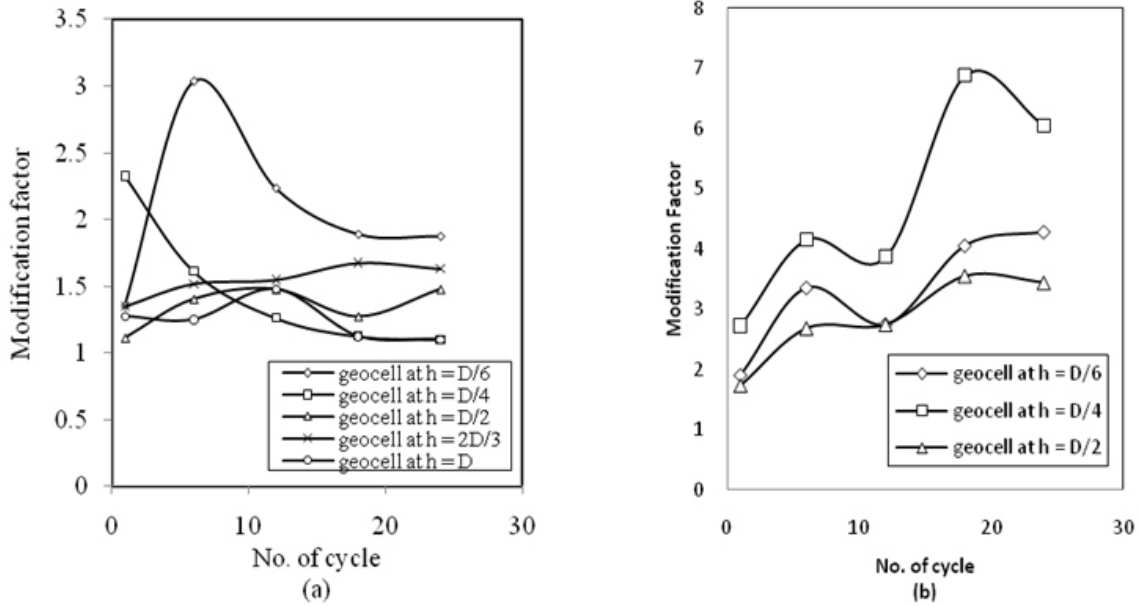


Figure 14. Modification factor for secant shear modulus against number of cycles: (a) with confining pressure 100 kPa (b) without confining pressure.

Normally, the damping ratio is defined as the ratio of damping coefficient (c) to the critical damping coefficient (c_c), however, it can also be defined as the ratio of the area of the loop (A_{loop}) AEFGHA to the area of the triangle ($A_{triangle}$) ABC through the following equation:

$$\text{Damping ratio } (\zeta) = \frac{A_{loop}}{4 \times \pi \times A_{triangle}} \quad (1)$$

The definition is further explained in Fig. 9. Variation of damping ratio with number of loading cycles is shown in Figs. 15 (a) and (b) for confined and unconfined tests. From the figures it is clearly seen that under a confining pressure of 100 kPa the damping ratio of unreinforced clay lies between 5 to 6.5% up to 25 numbers of loading cycles; whereas, with geocell reinforcement, the damping ratio reduces to 2 to 4% for the same number of loading cycles. However, a high damping ratio is observed for unconfined and unreinforced soil sample. Fig. 15 (b) shows that the damping ratio of unreinforced soft clay increases to 20% after 25 numbers of loading cycles under unconfined conditions. This implies that although soft clay has a property of amplifying the vibration amplitude, but with increase in loading cycles, the damping property of soft clay increases. This property of soft clay can be utilized in reducing the vibration amplitude by adopting soft clay dampers below the foundation [Singh and Dey, 2013].

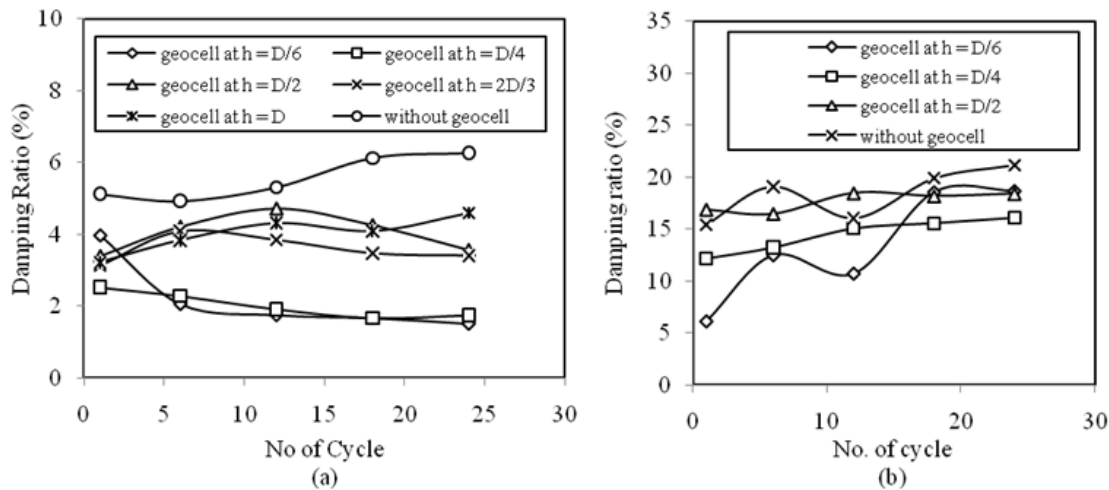


Fig.15 Damping ratio against number of cycle: (a) with confining pressure 100 kPa (b) without confining pressure.

In order to obtain the effect of geocells, modification factor of damping ratio is also calculated. From Figs. 16 (a) and (b) it is noted that with increase in number of cycles, geocell reinforcement reduces the modification factor under confined condition, but increases the modification factor under unconfined condition. Decrease in modification factor with number of cycles indicates that geocell reinforcement decreases the damping ratio with number of loading cycles. For unconfined condition the modification factor for damping ratio is around 0.8 after 25 numbers of loading cycles.

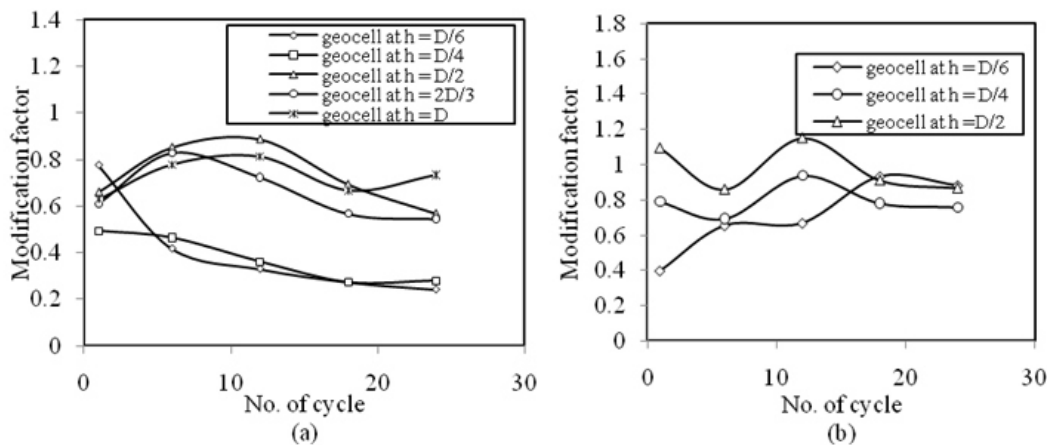


Figure 16 Modification factor for damping ratio against number of cycles: (a) with confining pressure 100 kPa (b) without confining pressure.

5. SUMMARY AND CONCLUSIONS

This paper has investigated the influence of geocell confinement on the strength and dynamic behaviours of soft clay. The deviatoric strength parameters were determined from the triaxial compression tests. The dynamic behaviours like damping ratio and secant shear modulus were

from cyclic triaxial tests. Effect of number of loading cycles and positions of geocell on degradation of deviatoric stress has been studied. The water content of the soft clay was tried to be maintained at 40%, near to the liquid limit of the soil. The following conclusions are drawn from the results of this investigation.

1. The induced apparent excessive strength depends on the position of the geocells from the top of the sample. It is observed that when the geocells are placed at one fourth of the diameter /width of the loading area, maximum benefit in strength is achieved.
2. Geocells reinforced soil does not show any failure stress under unconfined condition.
3. Position of geocells plays an important role on modification of properties of soft clay. Position of geocells under unconfined condition does not have any effect on gain in strength after a number of loading cycles.
4. There is a degradation of strength of soil after some loading cycles, however, the degradation is marginally less once geocells are inserted into the soil provided the geocells are not provided very close to the footing.
5. Lesser damping ratio and higher secant shear modulus are obtained if the soil is reinforced with geocells.
6. The secant shear modulus shows a maximum increase in its value under confined condition when geocells are placed at one-fourth of the loading diameter.
7. The improvement factor of deviatoric stress does not depend on the location of the geocells for unconfined conditions.
8. Under a confining pressure of 100 kPa the damping ratio of unreinforced clay lies between 5 to 6.5% upto 25 number of loading cycles; whereas, with geocell reinforcement, the damping ratio reduces to 2 to 4%. However, a high damping ratio of 20% is observed for unconfined and unreinforced soil samples.

REFERENCES

- [1] Bathurst, R.J., Karpurapu, R. 1993. Large scale triaxial tests on geocell reinforced granular soils. *Geotechnical Testing Journal* 16 (3), 296-303.
- [2] Bush, D.I., Jenner, C.G., Bassett, R.H., 1990. The design and construction of geocell foundation mattress supporting embankments over soft ground. *Geotextiles and Geomembranes* 9, 83-98.
- [3] Cowland, J.W., Wong, S.C.K., 1993. Performance of a road embankment on soft clay supported on a geocell mattress foundation. *Geotextiles and Geomembranes* 12, 687-705.
- [4] Dash, S.K., Krishnaswamy, N.R., Rajagopal, K., 2001. Bearing capacity of strip footings supported on geocell-reinforced sand. *Geotextiles and Geomembranes* 19, 235–256.
- [5] Dash, S.K., Rajagopal, K., Krishnaswamy, N.R., 2001b. Strip footing on geocell reinforced sand beds with additional planar reinforcement. *Geotextiles and Geomembranes* 19, 529–538.
- [6] Dash, S.K., Sireesh, S., Sitharam, T.G., 2003. Model studies on circular footing supported on geocell reinforced sand underlain by soft clay. *Geotext. Geomembr.* 21 (4), 197-219.
- [7] Fakher, A., Jones, C.J.F.P., 1996. Discussion of bearing capacity of rectangular footings on geogrid reinforced sand, by Yetimoglu, T., Wu, J.T.H., Saglamer, A.J. *Geotech. Eng. ASCE* 122 (4), 326e327.
- [8] Hendricker, A.T., Fredianelli, K.H., Kavazanjian, Jr., E., McKelvey III, J.A., 1998. Reinforcement requirement at a hazardous waste site. In: *Proc. of 6th Internat. Conf. On Geosynthetics, Atlanta, USA, Vol. 1*, pp. 465-468.
- [9] Leshchinsky, B., Ling, H., 2013. Effects of geocell confinement on strength and deformation behaviour of gravel. *J. Geotech. Geoenviron. Eng., ASCE* 139 (2), 340-352.
- [10] Madhavi, G.L., Vidya, S.M., 2007. Effects of reinforcement form on the behaviour of geosynthetic reinforced sand. *Geotext. Geomembr.* 25 (1), 23-32.
- [11] Rajagopal, K., Krishnaswamy, N.R., Latha, G.M., 1999. Behaviour of sand confined with single and multiple geocells. *Geotextiles and Geomembranes* 17, 171–184.
- [12] Seed, H.B., Idriss, I.M. 1971. Simplified procedure For evaluating soil liquefaction potential. *Soil Mech. Found. Div., ASCE* 107 (9), 1249-1274.
- [13] Selig, E.T., McKee, K.E., 1961. Static and dynamic behaviour of small footings. *J. Soil Mech. Found. Div. ASCE* 87 (6), 29e47.
- [14] Singha, S. and Dey, A.K. 2014. Dynamic properties of clay dampers. *National Seminar on Geotechnique Today - Prediction, Modelling & Construction, IGS, Kolkata chapter, Kolkata, Feb 28-March 1*, pp 141-146.

Trend Analysis of River Yamuna at Two Different Cities through Adaptive Neuro Fuzzy System

Shubhi Bhardwaj
ABES Engineering College, Ghaziabad, U.P

ABSTRACT

A river passes through many cities during its journey. The quality and purity of any river depend on many parameters such as number of industries, population density, air pollution and geographical location of the city it passes through. The present paper does an analysis on Yamuna River between two cities Delhi and Allahabad. The parameters in the analysis are Dissolved Oxygen (DO), Biochemical Oxygen Demand (BOD), Chemical Oxygen Demand (COD). These parameters are trained through Artificial Neuro Fuzzy Systems (ANFIS) and find a constant trend among several years. On the basis of trend found, the work can predict and calculate the size of the gap in next few years. The present paper also suggests the important parameters causing more pollution.

Keywords: - Dissolved Oxygen (DO), Biochemical Oxygen Demand (BOD), Chemical Oxygen Demand (COD), ANFIS

1. INTRODUCTION

Yamuna is one of the largest river in India. It is the largest tributary in North India.

Its total length is around 1370 kilometers. Yamuna originates from the Yamunotri Glacier of Uttarakashi in Uttar Pradesh. Yamuna flows through the states of Delhi, Haryana and Uttar Pradesh, before merging with the Ganges at Allahabad.

In Delhi, more than 70 per cent of Delhi's water supplies depend on the Yamuna and nearly 57 million people depend on the Yamuna waters. Yamuna is also the most polluted river in India. About 85% of the river's pollution comes from domestic household, municipal sites and industrial waste [2]. By the year 2025, two-thirds of the world's population will be facing water shortage. According to UN surveyed reports, India is expected to face critical levels of water stress by 2025 and there will be serious water shortages [2]. In this paper, data of three different parameters has been collected from different sources and then analysed through ANFIS.

Dissolved Oxygen (DO):- Dissolved oxygen analysis measures the amount of gaseous oxygen (O₂) dissolved in an aqueous solution. Oxygen gets into water by diffusion from the surrounding air, by aeration (rapid movement), and as a waste product of photosynthesis. As dissolved oxygen levels in water drop below 5.0 mg/l, aquatic life is put under stress. The lower the concentration, the greater the stress. Oxygen levels that remain below 1-2 mg/l for a few hours can result in large fish kills.

Biochemical Oxygen Demand (BOD):- Biochemical oxygen demand, or BOD, measures the amount of oxygen consumed by microorganisms in decomposing organic matter in stream water. BOD also measures the chemical oxidation of inorganic matter (i.e., the extraction of oxygen from water via chemical reaction).

Chemical Oxygen Demand (COD):- [Chemical oxygen demand \(COD\) is a measure of the capacity of water to consume oxygen during the decomposition of organic matter and the oxidation of inorganic chemicals such as ammonia and nitrite.](#)

Objective

The present paper has the following objectives:-

1. To identify the important parameter of water quality.
2. To train the datasets of parameter and observe a trend.
3. To check the status of parameter.

Hypothesis

The quality of water is highly depend on three parameter:-

1. Dissolved Oxygen (DO),
2. Biochemical Oxygen Demand (BOD),
3. Chemical Oxygen Demand (COD)

Methodology

The present work uses the data of different parameters and observe a trend in them .The important attributes that may affect the water quality of river are Dissolved Oxygen (DO), Biochemical Oxygen Demand (BOD), Chemical Oxygen Demand (COD).

The steps of the present work are:-

1. To identify the important parameter of water quality

The three main parameter data has been collected through several sites.A sample list is shown in table 1 and table 2

2. To train the datasets of parameter and observe a trend.

ANFIS is adaptive neuro fuzzy inference system, it combines the features of neural network and fuzzy logic principle. ANFIS is a hybrid learning algorithm. It is based on Sugeno-Takagi fuzzy inference system.

ANFIS(matlab toolbox)is used to train and test the data.The data is divided into two parts training and testing respectively.Training error is calculated at a fixed error and further testing is done the fixed training error.See figure 1 and figure2 .

3. To check the status of parameter.

On the basis of the training error,testing error is calaculated for each data.

Result

The comparison between two cities(fig 3) and(fig 4) shows the difference between their parameters.In fig 3 the drinking water pollution and inaccessibility is high than the Allahabad but the water pollution in Allahabad is more than in delhi. Drinking Water Quality and Accessibility is low in delhi than the Allahabad but the water quality in delhi is high than the Allahabad.

In fig4 the four different testing error is compared

Conclusion

Yamuna which acts as the life line for the majorities of cities has becomes polluted day by day.As many government agencies and and non government organisation have started many programmes for Yamuna water purity but due to non awareness in people as they throw plastic bags,garbage and industrial waste into the river make Yamuna more polluted.The possible way to make Yamuna clean is to aware people how much Yamuna and all other rivers are important for our future.Some guidelines ang regulation are also important such as ban on throwing waste material and industrial waste into Yamuna.

References

1. Biba Jasmine Kaur, George. M.P, Sandeep Mishra, ” Water quality assessment of river Yamuna in Delhi stretch during Idol immersion ”, INTERNATIONAL JOURNAL OF ENVIRONMENTAL SCIENCES Volume 3, No 6, 2013.

2. Darshan Malik^{1*}, Sunita Singh¹, Jayita Thakur¹, Raj Kishore Singh²,

Amarjeet Kaur², and Shashi Nijhawan¹, " Heavy Metal Pollution of the Yamuna River: An Introspection, ISSN: 2319-7706

Volume 3 Number 10 (2014) pp. 856-863

3. Mamta Rani, Pratima Akolkar, H.S. Bhamrah, " Water quality assessment of River Yamuna from origin to confluence to River Ganga, with respect to Biological water quality and Primary Water Quality Criteria.

4. WATER QUALITY DATA FOR RIVER YAMUNA

5. Anil Kumar Misra, " A River about to Die: Yamuna ", J. Water Resource and Protection, 2010, 2, 489-500

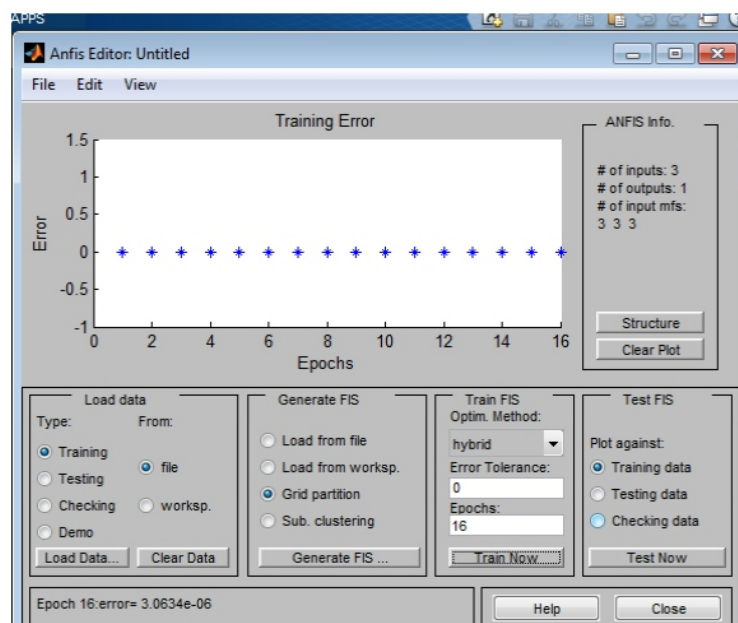
Table 1:-Sample Data For delhi

DO(mg/l)	BOD(mg/l)	COD(mg/l)
0.30	25	30
0.00	35	25
0.00	5	40
4.00	14	39
0.00	23	40

Table 2:-Sample Data For Allahabad

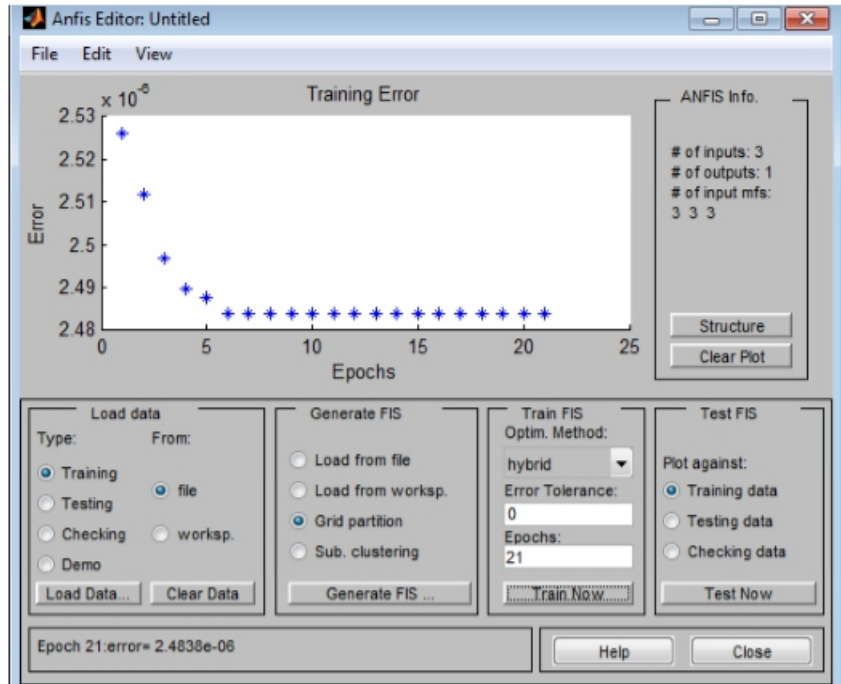
DO(mg/l)	BOD(mg/l)	COD(mg/l)
11.36	1.50	39.5
8.05	1.50	6.8
8.50	1	78.9
6.50	1.70	33.9
8.6	1.8	34.6

Fig 1:- Computed training error for delhi



Training Error at epoch 10 is 3.0634e-06

Fig 2:- Computed training error for Allahabad



Training Error at epoch 21 is 2.4838×10^{-6}

Figure 3:- Comparison of pollution parameters between delhi and Allahabad

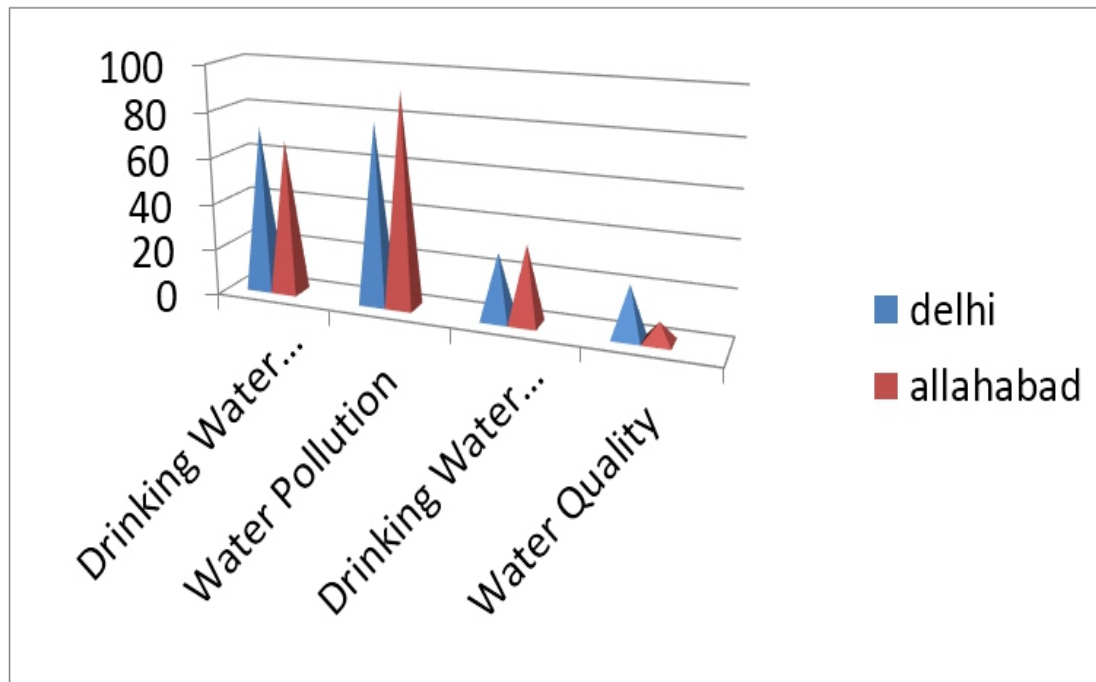
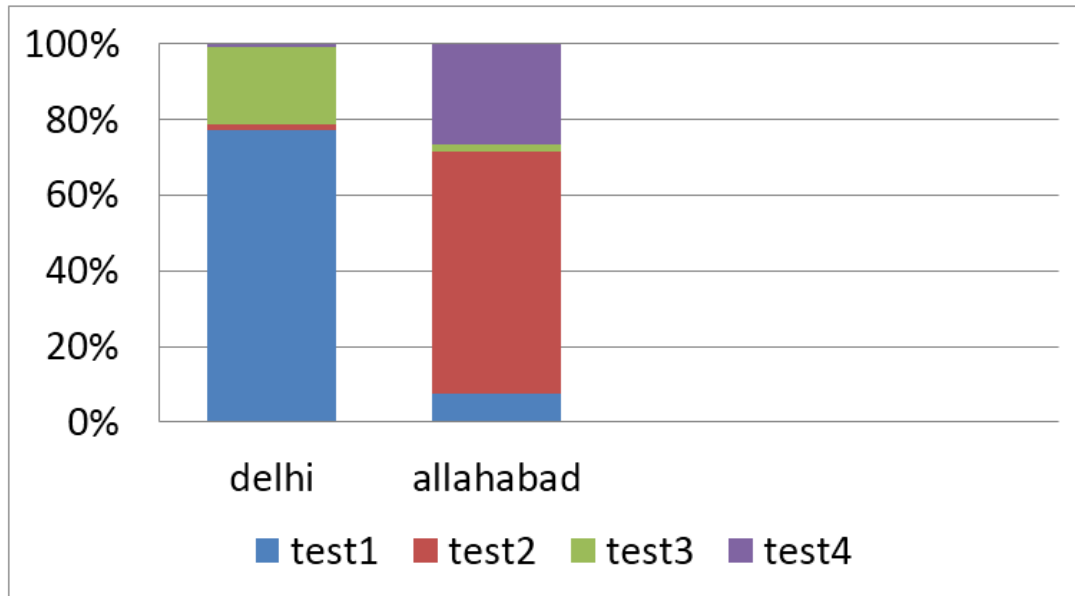


Figure 4:- Comparison on the basis of testing data



Instructions for Authors

Essentials for Publishing in this Journal

- 1 Submitted articles should not have been previously published or be currently under consideration for publication elsewhere.
- 2 Conference papers may only be submitted if the paper has been completely re-written (taken to mean more than 50%) and the author has cleared any necessary permission with the copyright owner if it has been previously copyrighted.
- 3 All our articles are refereed through a double-blind process.
- 4 All authors must declare they have read and agreed to the content of the submitted article and must sign a declaration correspond to the originality of the article.

Submission Process

All articles for this journal must be submitted using our online submissions system. <http://enrichedpub.com/> . Please use the Submit Your Article link in the Author Service area.

Manuscript Guidelines

The instructions to authors about the article preparation for publication in the Manuscripts are submitted online, through the e-Ur (Electronic editing) system, developed by **Enriched Publications Pvt. Ltd.** The article should contain the abstract with keywords, introduction, body, conclusion, references and the summary in English language (without heading and subheading enumeration). The article length should not exceed 16 pages of A4 paper format.

Title

The title should be informative. It is in both Journal's and author's best interest to use terms suitable. For indexing and word search. If there are no such terms in the title, the author is strongly advised to add a subtitle. The title should be given in English as well. The titles precede the abstract and the summary in an appropriate language.

Letterhead Title

The letterhead title is given at a top of each page for easier identification of article copies in an Electronic form in particular. It contains the author's surname and first name initial .article title, journal title and collation (year, volume, and issue, first and last page). The journal and article titles can be given in a shortened form.

Author's Name

Full name(s) of author(s) should be used. It is advisable to give the middle initial. Names are given in their original form.

Contact Details

The postal address or the e-mail address of the author (usually of the first one if there are more Authors) is given in the footnote at the bottom of the first page.

Type of Articles

Classification of articles is a duty of the editorial staff and is of special importance. Referees and the members of the editorial staff, or section editors, can propose a category, but the editor-in-chief has the sole responsibility for their classification. Journal articles are classified as follows:

Scientific articles:

1. Original scientific paper (giving the previously unpublished results of the author's own research based on management methods).
2. Survey paper (giving an original, detailed and critical view of a research problem or an area to which the author has made a contribution visible through his self-citation);
3. Short or preliminary communication (original management paper of full format but of a smaller extent or of a preliminary character);
4. Scientific critique or forum (discussion on a particular scientific topic, based exclusively on management argumentation) and commentaries. Exceptionally, in particular areas, a scientific paper in the Journal can be in a form of a monograph or a critical edition of scientific data (historical, archival, lexicographic, bibliographic, data survey, etc.) which were unknown or hardly accessible for scientific research.

Professional articles:

1. Professional paper (contribution offering experience useful for improvement of professional practice but not necessarily based on scientific methods);
2. Informative contribution (editorial, commentary, etc.);
3. Review (of a book, software, case study, scientific event, etc.)

Language

The article should be in English. The grammar and style of the article should be of good quality. The systematized text should be without abbreviations (except standard ones). All measurements must be in SI units. The sequence of formulae is denoted in Arabic numerals in parentheses on the right-hand side.

Abstract and Summary

An abstract is a concise informative presentation of the article content for fast and accurate Evaluation of its relevance. It is both in the Editorial Office's and the author's best interest for an abstract to contain terms often used for indexing and article search. The abstract describes the purpose of the study and the methods, outlines the findings and state the conclusions. A 100- to 250-Word abstract should be placed between the title and the keywords with the body text to follow. Besides an abstract are advised to have a summary in English, at the end of the article, after the Reference list. The summary should be structured and long up to 1/10 of the article length (it is more extensive than the abstract).

Keywords

Keywords are terms or phrases showing adequately the article content for indexing and search purposes. They should be allocated heaving in mind widely accepted international sources (index, dictionary or thesaurus), such as the Web of Science keyword list for science in general. The higher their usage frequency is the better. Up to 10 keywords immediately follow the abstract and the summary, in respective languages.

Acknowledgements

The name and the number of the project or programmed within which the article was realized is given in a separate note at the bottom of the first page together with the name of the institution which financially supported the project or programmed.

Tables and Illustrations

All the captions should be in the original language as well as in English, together with the texts in illustrations if possible. Tables are typed in the same style as the text and are denoted by numerals at the top. Photographs and drawings, placed appropriately in the text, should be clear, precise and suitable for reproduction. Drawings should be created in Word or Corel.

Citation in the Text

Citation in the text must be uniform. When citing references in the text, use the reference number set in square brackets from the Reference list at the end of the article.

Footnotes

Footnotes are given at the bottom of the page with the text they refer to. They can contain less relevant details, additional explanations or used sources (e.g. scientific material, manuals). They cannot replace the cited literature.

The article should be accompanied with a cover letter with the information about the author(s): surname, middle initial, first name, and citizen personal number, rank, title, e-mail address, and affiliation address, home address including municipality, phone number in the office and at home (or a mobile phone number). The cover letter should state the type of the article and tell which illustrations are original and which are not.

Address of the Editorial Office:

Enriched Publications Pvt. Ltd.
S-9, IInd FLOOR, MLU POCKET,
MANISH ABHINAV PLAZA-II, ABOVE FEDERAL BANK,
PLOT NO-5, SECTOR -5, DWARKA, NEW DELHI, INDIA-110075,
PHONE: - + (91)-(11)-45525005